Elastic and Rigidified CENP-A Nucleosomes govern Centromeric Chromatin Plasticity

Daniël P. Melters[1,*], Tatini Rakshit[1,*], Mary Pitman[1,2], Sergei A. Grigoryev[3], Minh Bui[1], David Sturgill[1], Garegin A. Papoian[2], and Yamini Dalal[1,#]

1 National Cancer Institute, Center for Cancer Research, Laboratory of Receptor Biology and Gene Expression, Bethesda, MD

2 University of Maryland, Department of Chemistry and Biochemistry, College Park, MD

3 Pennsylvania State University, College of Medicine, Hershey, PA

* Contributed equally

Corresponding author: dalaly@mail.nih.gov

Summary

At the heart of the centromere is the histone H3 variant CENP-A/CENH3, which seeds the kinetochore, creating the physical interface between chromosomes and mitotic spindles. How the kinetochore proteins modify CENP-A nucleosome dynamics *in vivo* is unknown. Here, using interdisciplinary analyses, we provide evidence suggesting that two structurally distinct CENP-A domains co-exist in human cells. One population sediments lighter, wraps DNA loosely, lacks kinetochore components, has diminished nucleosomal dimensions, and is more elastic than H3 nucleosomes. In contrast, the second population sediments heavier, strongly associates with inner kinetochore components, possesses stabilized octameric properties, and is more rigid than H3 nucleosomes. Dissecting the function of the elastic population suggests a role in maintaining an open chromatin environment permissive for RNAP2 occupancy and new CENP-A loading.

Shifting the balance between the two populations by overexpressing CENP-C results in suppression of centromeric chromatin plasticity.

Introduction

At the base of the inner kinetochore sits the histone H3 variant CENP-A/CENH3, which is marked by its rapid evolution (Malik & Henikoff 2001; Talbert et al 2004; Cooper & Henikoff 2004; Meraldi et al 2006; Maheshwari et al 2015). Despite lack of sequence conservation at the level of CENP-A or its associated DNA (Melters et al 2013), in most species, CENP-A chromatin provides the epigenetic and structural foundation by recruiting a triad of inner kinetochore proteins: CENP-B, CENP-C, and CENP-N (Régnier et al 2005; Carroll et al 2010; Mendiburo et al 2011; Pesenti et al 2016). Deleting either CENP-A or CENP-C results in cell death or induces senescence (Fukagawa et al 1999; Kwon et al 2007; McKinley & Cheeseman 2016). This happens only after a few cell cycles, suggesting that both CENP-A and CENP-C are likely present in excess over that required to form a functional kinetochore for one cell cycle. Furthermore, CENP-A and CENP-C are long-lived proteins, guaranteeing faithful chromosome segregation even after their genes have been deleted (Kalitsis et al 1998; Howman et al 2000; Suzuki et al 2011; Bodor et al 2013; Smoak et al 2016). Thus, deciphering features of the inner kinetochore, composed of CENP-A and its closest bound partners, is a fundamental biological question.

In a landmark study, individual mitotic kinetochores were successfully isolated from yeast using FLAG-tagged outer kinetochore components as bait (Gonen et al 2012). This study predominantly reported on features of the outer kinetochore but were unable to dissect the unique

inner kinetochore-bound CENP-A nucleosome (Bloom & Carbon 1982; Furuyama & Henikoff 2009; Furuyama et al 2013; Díaz-Ingelmo et al 2015). In contrast, human centromeres reside on megabase-sized α-satellite arrays (Rudd et al 2006). Recent advances in super-resolution microscopy suggest that human centromeres contain ~400 CENP-A molecules (Bodor et al 2014), which eventually associate with ~17 mitotic spindle microtubules (Suzuki et al 2015). The field has made enormous strides in understanding how inner kinetochore components modulate CENP-A nucleosome dynamics *in vitro* (Kato et al 2013; Falk 2015 et al; Falk et al 2016; Guo et al 2017; Chittori et al 2018; Pentakota et al 2018). In contrast, how the inner kinetochore complex structurally affects CENP-A nucleosomes *in vivo* remains an open question.

In this report, we dissect properties of human centromeric chromatin bound to the inner kinetochore complex *in silico*, *in vitro*, and *in vivo.* First, using computational modeling, we find that CENP-C diminishes conformational flexibility of the CENP-A nucleosome. Next, applying pushing forces by nano-indentation, we demonstrate that *in vitro*, CENP-A nucleosomes are elastic relative to H3 nucleosomes, but remarkably lose this elasticity when bound to CENP-C. Next, using a purification scheme to obtain native inner kinetochore complexes, we observe two distinct classes of CENP-A nucleosomes co-exist *in vivo*. One class of CENP-A nucleosomes is not enriched in inner kinetochore proteins, sediments in the lighter fractions of glycerol gradients, has looser associations with DNA, and possesses smaller dimensions; whereas, another class of CENP-A nucleosomes co-elute and co-purify with inner kinetochore proteins, have tighter interactions with DNA, and possess octameric dimensions. Finally, we dissect a potential function for elastic CENP-A population, finding that its loss impacts the plasticity of

centromeric chromatin, suppressing access to the transcriptional machinery and *de novo* CENP-A incorporation. These data support a model in which a balance between elastic and rigid CENP-A domains regulate centromeric chromatin plasticity *in vivo*.

Results

Work from various groups has shown that CENP-A nucleosomes are dynamic (Chen et al 2003; Fujita et al 2007; Conde e Silva et al 2007; Dalal et al 2007; Williams et al 2009; Bui et al 2012; Wisniewski et al 2014; Kono et al 2015; Stumme-Diers et al 2018). In contrast, data also suggests that CENP-A nucleosomes are highly rigid relative to canonical H3 nucleosomes *in vitro* (Black et al 2004; Black et al 2007; Sekulic et al 2010; Panchencko et al 2011). Upon binding either CENP-C or CENP-N, CENP-A nucleosome dynamics are altered (Kato et al 2013; Falk et al 2015; Falk et al 2016; Guo et al 2017; Chittori et al 2018; Pentakota et al 2018). Indeed, given the unique requirements for fidelity that CENP-A chromatin provides *in vivo* during replication, transcription, and mitosis (Bloom 2008), whether they are structurally rigid, or elastic remains a fundamental question. To gain insights into this problem, we first performed computational modeling to assess what happens to CENP-A nucleosomes when bound to CENP-C.

Modeling CENP-A:CENP-C^{CD} nucleosomes predicts a change in conformational flexibility

Previous computational modeling demonstrated that CENP-A nucleosomes have an intrinsically more distortable nucleosome core, compared to H3 nucleosomes (Winogradoff et al 2015). The corresponding free energy landscape predicts the existence of multiple conformational states of CENP-A. Here, we carried out all-atom explicit-solvent molecular dynamics simulations, from

which we obtained the free energy landscapes of CENP-A nucleosomes, with, or without the central domain fragment of CENP-C (CENP-C^{CD}). Strikingly, in the presence of CENP-C^{CD}, the otherwise rugged free energy landscape of CENP-A nucleosomes collapses into just two broad basins (Figure 1A), with a distribution similar to that of H3 (Winogradoff et al 2015). This change in the free energy landscape manifested itself in the loss of the bimodal distribution of the movements of the center of mass (Figure S1A). Furthermore, local structural flexibility was also suppressed upon CENP-C^{CD} binding (Figure S1B). Overall, these findings indicate that CENP-C^{CD} limits the conformational distortability and motions of CENP-A nucleosomes.

CENP-A nucleosomes are highly elastic, a property that is lost upon CENP-C^{CD} binding

We set out to experimentally test these modeling results, which predict that CENP-A nucleosomes are elastic, and should lose elasticity upon CENP-C^{CD} binding. Stiffness of materials is measured by the ratio of stress (N/m^2 or Pascal) to strain (indentation), known as the Young's modulus. In physics and biology, nano-indentation experiments are a well-accepted means of measuring the physical properties of biological materials (Vinckier & Semenza 1998; Rakshit et al 2013).

Despite the longstanding use of nanomechanical force spectroscopy, we were surprised to discover that the elasticity of nucleosomes has never been reported. Therefore, we performed in-fluid, single-molecule, nano-indentation force spectroscopy (Heinz & Hoh 1999; Butt et al 2005). We first measured the nucleosomal dimensions of H3 and CENP-A *in vitro* reconstituted arrays under physiological conditions. As reported earlier (Walkiewicz et al 2014; Athwal et al 2015), we found that *in vitro* reconstituted CENP-A nucleosomes possess dimensions similar to

H3 nucleosomes (3.7±0.3 and 3.8±0.3 nm, resp.) (Table S1). Next, we performed in-fluid nano-indentation on these reconstituted nucleosomes (Figure 1B). H3 nucleosomes had a Young's modulus of 11.1±4.5 MPa; strikingly, CENP-A nucleosomes were nearly twice as elastic (6.2±3.9 MPa) (Figure 1C-E, Table S2).

We were curious whether CENP-C^{CD} would suppress CENP-A nucleosomal elasticity. First, we measured the dimensions of CENP-C^{CD} bound to CENP-A nucleosomes, finding that they are slightly taller than CENP-A nucleosomes alone (3.7±0.3 nm vs. 4.1±0.4 nm) (Table S1). Next, we measured the elasticity. About half the CENP-A nucleosomes remained highly elastic (5 MPa), whereas the other half lost elasticity by a factor of three (14.5 MPa) (1-way ANOVA $P<0.0001$) (Figure 1D, E, Table S2). This bimodal distribution of the CENP-A+CENP-C^{CD} population most likely represents two distinct CENP-A sub-species: one free (5 MPa), and the other bound to CENP-C^{CD} (14.5 MPa). We next assessed whether these properties might also translate into distinct CENP-A domains *in vivo*.

Two distinct CENP-A populations co-exist *in vivo*

To test the hypothesis that two populations of CENP-A nucleosomes co-exist *in vivo*, we developed a gentle purification assay (Figure S2) to separate CENP-C associated chromatin from CENP-A chromatin using serial native chromatin immunoprecipitation (N-ChIP) (Figure 2A). Prior to N-ChIP, we mildly digested nuclear chromatin with micrococcal nuclease (MNase), and size-separated the extracted chromatin on a glycerol gradient. This protocol resulted in a wide variety of nucleosome arrays (Figure 2B). A Coomassie stain confirmed that fractions 2-12 contained bulk histones (Figure 2C).

We next performed CENP-C N-ChIP and analyzed these samples by western blot to detect CENP-C and CENP-A (Figure 2D). While a small amount of CENP-A/CENP-C ran in the lighter fraction, the vast majority of CENP-C-bound CENP-A complexes migrated in larger chromatin arrays (fraction 12). To pull down any remaining CENP-A protein, we used ACA serum (Moroi et al 1980; Earnshaw & Rothfield 1985), which contains anti-centromere antibodies. In contrast to CENP-C N-ChIP, virtually no remaining CENP-C was detected in the serial ACA N-ChIP, but CENP-A mononucleosomes were pulled down (Figure 2E). In short, the pattern of CENP-A detected following either CENP-C N-ChIP or serial ACA N-ChIP was very distinct (Figure 2F).

We were curious whether both CENP-A populations derive from the same centromeric sequences. Therefore, we performed ChIP-seq on CENP-C and serial ACA samples using the PacBio sequencing platform. These analyses demonstrated that both fractions largely occupy identical centromeric sequences (Figure S3).

As noted above, the majority of CENP-A bound to CENP-C, was detected predominantly in fraction 12 (Figure 2D). This relative abundance of longer chromatin arrays in the CENP-C N-ChIP was also observed by high resolution capillary electrophoresis (BioAnalyzer, Figure S4). Altogether, the serial N-ChIP demonstrates that two distinct populations of CENP-A can be purified in succession from the same sample, supporting the hypothesis that two separable populations of native CENP-A co-exist *in vivo*.

A sub-fraction of CENP-A nucleosomes associates with the inner kinetochore

We quantified the relative abundance of CENP-A bound to CENP-C within our extracted chromatin samples (Figure 3A). The enrichment of the N-ChIP'ed sample was measured over the input (Figure 3B). CENP-A was enriched 4.4-fold (SE 0.9) in the CENP-C N-ChIP, whereas CENP-A was enriched 28.5-fold (SE 6.9) in the serial ACA N-ChIP (Figure 3C, Table S3; n=11 independent experiments). These data support the interpretation that CENP-A domains which are not strongly bound to CENP-C exist at centromeres.

Next, we interrogated the possibility that CENP-A nucleosomes associated with the inner kinetochore might contain other histone variants, most notably H2A variants, which were previously shown to co-purify with tagged CENP-A (Foltz et al 2006). We did not detect γH2A.X; in contrast, H2A.Z and macroH2A were detected in both CENP-C and serial ACA N-ChIP, but there was no significant difference between the two samples (Figure 3D, E, Table S4).

Notably, CENP-C N-ChIP, but not serial ACA N-ChIP, was enriched with inner kinetochore proteins CENP-T, CENP-W, CENP-I, and CENP-N (Figure 4A-C). Thus, our results indicate that in HeLa cells, stoichiometrically, there is an almost 6-fold excess of bulk CENP-A that is on centromeric DNA, but which does not robustly associate with inner kinetochore complexes.

Bulk CENP-A nucleosomes wrap DNA loosely, whereas CENP-C suppresses nucleosomal access

Nano-indentation force spectroscopy suggested that CENP-A nucleosomes are innately more elastic than H3 nucleosomes (Figure 1D). Therefore, we wondered if, *in vivo* CENP-A

nucleosomes had flexible DNA wrapping, and which might be altered by CENP-C associated complexes. Using the *in vivo* purified samples prepared as above (Figure 4A), we first assayed nucleosomal DNA accessibility using the combined nuclease activity of Exonuclease III and MNase. We found that the nucleosomal DNA ends of both CENP-A population was far more accessible compared to H3 particles (Figure S5). Next, we asked whether DNA wrapping around the nucleosome core was different. To examine this, we turned to the classical DNase I assay (Noll 1974), which only cuts at the exposed minor groove of the DNA double helix when wrapped around a nucleosome core. Canonical bulk mononucleosomes displayed the standard 10-bp ladder going up to 140-bp, whereas bulk CENP-A mononucleosomes displayed a hyper-accessible pattern consistent with underwound DNA (Figure 4D, E). In striking contrast, DNase I had limited access to CENP-C bound CENP-A nucleosomes (Figure 4D, E). We interpret these data to mean that the inner kinetochore stabilizes DNA that otherwise is loosely wrapped around CENP-A nucleosomes.

Physically taller CENP-A nucleosomes are bound to the inner kinetochore

We examined the characteristics of chromatin associated with CENP-C. In order to image these complexes, we split the samples in half, and imaged them by in-air AFM, or transmission electron microscopy (TEM) (Figure 5A-C, S6). The sedimentation assay (Figure 2D) informed us that there were multiple populations of CENP-C bound to chromatin. Therefore, we anticipated a heterogeneous population of complexes containing CENP-A:CENP-C. Indeed, by AFM and TEM, we observed large polygonal structures with a roughly circular footprint (height: 5.6±2.1 nm; width: 54.7±14.5 nm) associated with four to six nucleosomes (Figure 5B, S6, Table S5). Compared to individual nucleosomes these CENP-C complexes were substantially larger.

These structures were not observed in either mock IP, bulk chromatin, or CENP-A N-ChIP (Figure 5B, S6). Additionally, the largest of CENP-C complexes was associated with a ~230-bp long nucleosome-free DNA (Figure 5B, S6, Table S6). The same samples, analyzed in parallel by TEM, displayed similar features (Figure 5C, S6), including the association of four to six nucleosomes at the periphery of the CENP-C complex.

We next turned our attention to the nucleosomes associated with CENP-C. In our previous work, recombinant octameric CENP-A nucleosomes on 601 or α-satellite DNA behave similar to H3, with average heights of ~2.4 nm and widths of ~12 nm (Figure 1E; Walkiewicz et al 2014; Athwal et al 2015). This observation is consistent with a range of static measurements made by biophysical, EM, and crystallographic methods, which show that except for flexible exit/entry DNA termini and loop 1, *in vitro* reconstituted CENP-A nucleosomes behave similar to H3 nucleosomes (Tachiwana et al 2011; Walkiewicz et al 2014; Roulland et al 2016; Vlijm et al 2017).

In contrast, native CENP-A nucleosomes purified from either fruit fly or human cell lines display smaller dimensions compared to native H3 nucleosomes, except during S phase (Dalal et al 2007; Dimitriadis et al 2010; Bui et al 2012; Bui et al 2013; Athwal et al 2015). Indeed, we recapitulated these observations here. Relative to H3 nucleosomes (2.5±0.3 nm) (Figure 5D, Table S7), native bulk CENP-A nucleosomes alone are uniquely identifiable by a smaller average height of 1.9±0.3 nm (Figure 5D). We next examined CENP-A nucleosomes associated with CENP-C complexes (Figure 5D, S6, Table S7). To our surprise, these nucleosomes were

octameric in height (Figure 5D), with a height of 2.4±0.5 nm, and significantly taller (t-test $p<0.001$) than CENP-A nucleosomes alone.

Immuno-AFM confirms presence of CENP-A nucleosomes within CENP-C complexes

To confirm the identity of the octameric nucleosomes associated with CENP-C, we devised a single-molecule based method to test whether CENP-A nucleosomes are physically present in CENP-C N-ChIP samples. Similar to immuno-EM protocols, in which one can confirm the identity of a given molecule, we adapted immuno-labeling for in-air AFM (Figure 6A). We first visualized either without antibody; or, 1° mouse monoclonal anti-CENP-A antibody; or, 1° CENP-A antibody and, either 2° anti-mouse antibody or 2° anti-mouse Fab fragment. The 1° antibody by itself was 0.8±0.2 nm in height and the addition of the 2° antibody resulted in a height increase to 2.0±0.5 nm (Figure 6B, C, Table S8, S9). To confirm the 1° antibody's specificity, we *in vitro* reconstituted recombinant H3 or CENP-A nucleosomes as before (Figure 1B, 6A), and incubated them with either no antibody; 1°; or, 1° and 2° antibodies (Figure 6B, C, S7). Whereas *in vitro* reconstituted H3 nucleosomes did not show a shift in particle height in the presence of anti-CENP-A antibodies (no: 2.2±0.2nm, 1°: 2.1±0.2 nm, and 2°: 2.2±0.1 nm, resp.). As expected, these *in vitro* reconstituted CENP-A nucleosomes did increase in height (no: 2.2±0.2 nm, 1°: 2.5±0.3 nm, and 2°: 4.6±1.4 nm, or Fab: 3.2±0.6 nm, resp.).

Next, we applied the same method to native H3 or CENP-C purified complexes (Figure 6B, C). Similar to reconstituted H3 nucleosomes, bulk H3 chromatin did not shift in particle height when incubated with anti-CENP-A antibodies (no: 2.3±0.2 nm, 1°: 2.4±0.3 nm, and 2°: 2.3±0.1 nm, resp.). In contrast, nucleosomal particles that came down in the CENP-C N-ChIP displayed a

shift in height when challenged with anti-CENP-A antibodies (no: 2.4±0.4 nm, 1°: 2.6±0.4 nm, and 2°: 3.9±1.3 nm, resp.). These results lend confidence to the interpretation that CENP-A nucleosomes are associated with the purified CENP-C complex.

These results suggest the presence of two physically distinct CENP-A nucleosomes within the human centromere: one species of shorter CENP-A nucleosomes, and one octameric species of CENP-A nucleosome associated with a CENP-C complex.

Altering the balance between flexible and rigid CENP-A domains changes chromatin plasticity

Cumulatively, the data above suggest that one type of structure in the inner kinetochore is comprised of a polygonal dome-like structure with a roughly circular footprint, associated with a chromatin sub-domain comprised of four to six octameric CENP-A nucleosomes. Yet another type of domain in the centromere contains smaller, flexible CENP-A nucleosomes that encode an open chromatin state. We next sought to dissect a function for the shorter CENP-A population.

We first hypothesized that during mitosis smaller CENP-A particles might provide a mechanical "bungee"-like state, which allows the dissipation of mitotic forces. In this scenario, we postulated, excess CENP-C would dampen the motions of CENP-A (Figure 1A), thereby reducing the overall springiness of centromeric chromatin; and loss of the flexible CENP-A domain might result in an accumulation of DNA breaks during mitosis. To test this hypothesis, we overexpressed C-terminally tagged GFP CENP-C (OE) for three days, in cells synchronized to late mitosis and early G1 (Figure 7A) and scored for the DNA break marker γH2A.X.

Although we do observe an increase in mitotic defects, no appreciable increase in γH2A.X was observed at centromeric foci (Figure S8). These data would, a priori, rule out the hypothesis that flexibility of CENP-A plays a direct role in dissipation of mitotic tension.

A second hypothesis we considered was whether the flexible CENP-A domain provides an open chromatin state, permissive to transcription. In this scenario, we postulated, excess CENP-C should shut down the open chromatin state, thereby inhibiting the transcriptional machinery, namely, RNA polymerase 2 (RNAP2).

To test this hypothesis, we first computationally examined the effect of doubling the amount of CENP-C per CENP-A nucleosome. Compared to a single CENP-C^{CD} fragment, binding two CENP-C^{CD} fragments globally reduced whole histone motions and local residue fluctuations of CENP-A nucleosomes (Figure S9A, B). Next, we assessed DNA gyre sliding and gaping motions within the CENP-A nucleosome. We modeled these motions using the same residues as in previous smFRET experiments (Falk et al 2016). This high-resolution analysis showed that a single CENP-C^{CD} fragment dampens the CENP-A nucleosome gyre gaping; where DNA slides asymmetrically away from the CENP-C bound-face of CENP-A nucleosomes. In contrast two CENP-C^{CD} fragments freeze both gaping and sliding motions (Figure 7B, S9C). One prediction from these modeling data is that increasing CENP-C concentration should dampen CENP-A nucleosomal plasticity.

To examine these predictions, we turned to our *in vitro* reconstitution system for measuring elasticity. Here, we doubled the concentration of CENP-C^{CD} fragment (Figure 7B, from 2.2X to

4X) relative to CENP-A nucleosomes. As demonstrated above (Figure 1D), addition of the standard 2X molar excess of CENP-C^{CD} to reconstituted CENP-A nucleosome arrays resulted in a bimodal distribution of elasticity (Figure 7C). However, when we doubled CENP-C excess, virtually all CENP-A nucleosomes lose elasticity, and become rigidified (17.1±10.6 MPa, Figure 7C, Table S10).

One potential outcome of loss of nucleosome elasticity is the potential for chromatin clustering or compaction. Indeed, we noticed a qualitative increase in *in vitro* reconstituted CENP-A nucleosome clustering when exposed to CENP-C in a dose-dependent manner (Figure S10A). We were extremely curious to know if we could induce CENP-A chromatin compaction by simply by adding recombinant CENP-C^{CD} fragment to native ACA N-ChIP samples. Indeed, we observed a ~30% increase in chromatin compaction upon the addition of CENP-C^{CD}. One logical outcome from these results is that excess CENP-C encodes a centromeric fiber that is less permissive to chromatin binding factors, for instance, transcriptional machinery.

We tested this hypothesis by overexpressing CENP-C *in vivo* for three days, after which we purified centromeric chromatin as above (Figure 3A). We first assessed whether overexpression of CENP-C would also induce CENP-A chromatin compaction *in vivo*. We purified ACA CENP-A chromatin and measured compaction as above. We observed a doubling of compacted chromatin states relative to controls (Figure 7D, S10A, Table S11). We next measured the nucleosomal dimensions of the CENP-C bound CENP-A nucleosomes, and of bulk CENP-A nucleosomes. In cells overexpressing CENP-C, bulk CENP-A nucleosomes displayed a marked increase in particle height (2.0±0.5 nm vs 3.5±0.8 nm, resp. Figure S10B, Table S12). These data

suggest that in the CENP-C overexpression background, there is not only enhanced clustering/compaction of nucleosomes, but also a general shift towards suppression of plasticity of individual CENP-A nucleosomes.

During late mitosis and early G1, RNAP2 is present at the centromere (Müller & Almouzni 2017). We wondered whether overexpression of CENP-C, and the creation of more closed conformation of CENP-A chromatin, would lead to reduced accessibility for RNAP2. Indeed, by western blot analysis, when CENP-C is overexpressed we observed a significant reduction in RNAP2 at both CENP-A domains (3- and 2-fold reduction, resp.; t-test $p<0.05$; Figure 7E, Table S13). Additionally, we only observed a loss of bulk CENP-A when CENP-C was overexpressed (t-test $p<0.05$; Figure 7E, Table S13). Likewise, co-IF for CENP-A and RNAP2 on chromatin fibers extracted from cells, demonstrated reduction of RNAP2 occupancy on centromeric fibers when CENP-C is overexpressed (Figure S11).

Work from several labs have recently suggested that transcription of centromeric DNA is required for *de novo* CNEP-A loading. (Müller & Almouzni 2017). In this scenario, overexpression of CENP-C, which suppressed RNAP2 at centromeres (Figure 7E), should also lead to reduced de novo CENP-A loading. To test this idea, we turned to the well-established SNAP-tagged CENP-A system combined with quench pulse-chase immunofluorescence (Bodor et al 2013) to track *de novo* integrated CENP-A. Strikingly, in the CENP-C overexpression background, we observed a 2.3-fold reduction of de novo incorporation of CENP-A (t-test $p<0.01$; Figure 7F, Table S14).

Taken together, these data suggest that flexible CENP-A nucleosomes create an open chromatin environment, whereas CENP-C rigidifies a small subset of CENP-A nucleosomes and fixes these in an octameric state. Innately flexible CENP-A nucleosomes, in contrast, encode a more open chromatin fiber, which permit RNAP2 occupancy, a property that is diminished upon even moderate overexpression of CENP-C, resulting in reduced loading of new CENP-A (Figure 7G).

Discussion

Since the discovery of CENP-A (Earnshaw & Rothfield 1985; Palmer et al 1991) it has been recognized that CENP-A nucleosomes are required and sufficient to form kinetochores (Régnier et al 2005; Mendiburo et al 2011). A conundrum is that more CENP-A nucleosomes reside at the centromere than are strictly needed to successfully seed a kinetochore (Bodor et al 2013; McKinley & Cheeseman 2016). Previous work has shown that *in vitro,* both the central domain and the conserved CENP-C motif contact the CENP-A C-terminal tail and latch on the H2A acidic patch (Kato et al 2013). In smFRET experiments of *in vitro* reconstituted CENP-A mononucleosomes, these contacts showed restricted DNA gyre gapping and sliding (Falk et al 2015; Falk et al 2016; Guo et al 2017).

One hypothesis arising from our previous (Winogradoff et al 2015), and current modeling experiments, is that CENP-A nucleosomes can intrinsically sample altered nucleosome conformations and, are structurally "frustrated"; but binding by kinetochore components chooses- and fixes- one specific conformational state. Indeed, when we modeled CENP-A nucleosomes alone, vs. those bound to CENP-C^{CD}, we observed both, a marked diminution of motion, and free energy minima, representing lost conformational flexibility (Figure 1A,7B, S1,

S9). The diminution of conformational flexibility correlates with a loss of elasticity of CENP-A nucleosomes upon CENP-C^{CD} binding. Indeed, this is what we observed *in vitro* (Figure 1D,7F). Taking these observations *in vivo,* we observe a shift in nucleosomal height of CENP-A nucleosomes when associated with CENP-C complexes (Figure 5D). One speculative interpretation of this shift is that *in vivo*, the CENP-C complex suppresses conformational flexibility, and stabilizes CENP-A nucleosomes in an octameric conformation.

Several important implications arise from our observations, including with regards to the ongoing debate surrounding the conformational and compaction status of CENP-A nucleosomes (which are discussed in detail in Supplementary Information).

A crucial question that emerges from our data is *why* CENP-A, but not H3, has evolved as a metastable histone variant. We speculate that elasticity of CENP-A may be a conserved intrinsic property which allows adaptable behaviors that help distinguish centromeric CENP-A from ectopic CENP-A (Lacoste et al 2014; Athwal et al 2015; Fang et al 2015; Müller & Almouzni 2017). Another possibility is that elastic CENP-A nucleosomes in the absence of its kinetochore partners are more susceptible to ejection from chromatin (Dalal et al 2007; Kim et al 2016). A third possibility is that elasticity of CENP-A contributes to the accessibility of the centromeric chromatin fiber, potentially by allowing nucleosomes to deform or slide more easily. Indeed, in support of this idea, overexpression of CENP-C resulted in decreased localization of RNAP2 at both CENP-A domains and correlates with the loss of *de novo* CENP-A loading (Figure 7).

Nucleosome dynamics play a critical role in genome compaction, protection from DNA damaging agents, and regulate DNA access to DNA binding complexes (Polach & Widom 1995; Widom 1998; Bowman & Poirier 2015). Recently, we described a CENP-A core posttranslational modification (PTM), which modulated binding of CENP-C *in vivo* (Bui et al 2017). An exciting line of future investigation is to examine how location, (i.e., DNA sequence), or core CENP-A PTMs, especially those at the histone-DNA and histone-histone interfaces, promote or weaken the CENP-A nucleosome, its interactions with kinetochore partners, and centromere satellite DNA. Intriguingly, centromere DNA and genes are rapidly evolving (Henikoff et al 2001; Melters et al 2013). Furthermore, not all species share all kinetochore components; centromeric genes are lost, duplicated, and sometimes invented (Ross et al 2013; Drinnenberg et al 2016; van Hooff et al 2017). Despite these evolutionary changes, the chromatin structure of centromeres must be maintained, to accomplish its fundamental function- and structure- during mitosis. Investigating whether CENP-A structures are conserved or co-evolve with kinetochore proteins, might provide clues into what drives the evolution of centromere chromatin, in turn serving as an excellent model for the evolution of epigenetic systems in the genome.

STAR methods

Detailed methods are provided in the online version of this paper and include the following

- Key resources table
- Contact for Reagent and Resource Sharing
- Experimental model and subject details
- Method details

- All-atom computational modeling
- Serial native chromatin immunoprecipitation
- Glycerol sedimentation assay
- AFM
- Immuno-AFM
- AFM Force Spectroscopy
- TEM
- ChIP-DNase I
- ChIP-exo
- Chromatin fiber immunofluorescence
- Immunostaining of mitotic chromosomes
- Quench chase immunostaining
- ChIP-seq

- Quantification and statistical analyses

Authors contribution

Conceptualization: D.P.M. and Y.D.; Methodology: D.P.M., T.R., S.A.G., M.P., M.B., D.S., and Y.D.; Investigation: D.P.M., T.R., M.P., M.B., D.S., and S.A.G.; Writing – original draft: D.P.M. and Y.D.; Writing – Review & Editing: D.P.M., T.R., S.A.G, G.A.P., and Y.D.; Funding Acquisition: S.A.G., G.A.P., and Y.D.; Visualization: D.P.M; Supervision: Y.D.

Acknowledgements

We thank Kerry Bloom for encouraging us to investigate kinetochore associated chromatin; Steve Henikoff for sharing cut-and-run CENP-C mapping results; Andrea Musacchio for feedback on an earlier version of this manuscript; Tom Misteli, Sam John, and members of our laboratory for critical comments; Will Heinz and Emilios Dimitriadis for discussions on force spectroscopy experiments; Stephan Diekmann and Dan Foltz for gifting GFP-CENP-C and SNAP-tagged CENP-A constructs, respectively. DPM, TR, MB, DS, and YD are supported by the Intramural Research Program of the Center for Cancer Research at the National Cancer Institute/NIH. MP is supported by the joint NCI-UMD Cancer Technology Partnership. GAP is supported by NSF grant CHE-1363081. SAG was supported by NSF grant 1516999.

References

Athwal, R.K., Walkiewicz, M.P., Baek, S., Fu, S., Bui, M., Camps, J., Ried, T., Sung, M.H. & Dalal, Y., 2015, CENP-A nucleosomes localize to transcription factor hotspots and subtelomeric sites in human cancer cells, *Epigenetics Chromatin*, 8, p. 2.

Black, B.E., Foltz, D.R., Chakravarthy, S., Luger, K., Woods, V.L. & Cleveland, D.W., 2004, Structural determinants for generating centromeric chromatin, *Nature*, 430(6999), pp. 578-82.

Black, B.E., Jansen, L.E., Maddox, P.S., Foltz, D.R., Desai, A.B., Shah, J.V., & Cleveland, D.W., 2007, Centromere identity maintained by nucleosomes assembled with histone H3 containing the CENP-A targeting domain, *Mol Cell*, 25(2):309-22.

Bloom, K.S., 2008, Beyond the code: the mechanical properties of DNA as they relate to mitosis, *Chromosoma*, 117(2):103-10.

Bloom, K.S. & Carbon, J., 1982, Yeast centromere DNA is in a unique and highly ordered structure in chromosomes and small circular minichromosomes, *Cell*, 29(2), pp. 305-17.

Bodor, D.L., Mata, J.F., Sergeev, M., David, A.F., Salimian, K.J., Panchenko, T., Cleveland, D.W., Black, B.E., Shah, J.V. & Jansen, L.E., 2014, The quantitative architecture of centromeric chromatin, *Elife*, 3, p. e02137.

Bodor, D.L., Valente, L.P., Mata, J.F., Black, B.E. & Jansen, L.E., 2013, Assembly in G1 phase and long-term stability are unique intrinsic features of CENP-A nucleosomes, *Mol Biol Cell*, 24(7), pp. 923-32.

Bowman, G.D. & Poirier, M.G., 2015, Post-translational modifications of histones that influence nucleosome dynamics, *Chem Rev*, 115(6), pp. 2274-95.

Bui, M., Dimitriadis, E.K., Hoischen, C., An, E., Quénet, D., Giebe, S., Nita-Lazar, A., Diekmann, S. & Dalal, Y., 2012, Cell-cycle-dependent structural transitions in the human CENP-A nucleosome in vivo, *Cell*, 150(2), pp. 317-26.

Bui, M., Pitman, M., Nuccio, A., Roque, S., Donlin-Asp, P.G., Nita-Lazar, A., Papoian, G.A. & Dalal, Y., 2017, Internal modifications in the CENP-A nucleosome modulate centromeric dynamics, *Epigenetics Chromatin*, 10, p. 17.

Bui, M., Walkiewicz, M.P., Dimitriadis, E.K. & Dalal, Y., 2013, The CENP-A nucleosome: a battle between Dr Jekyll and Mr Hyde, *Nucleus*, 4(1), pp. 37-42.

Butt, H.-J., Cappella, B., & Kappl, M., 2005, Force measurements with the atomic force microscope: technique, interpretation and application, *Surface Sci Rep*, 59:1-152.

Carroll, C.W., Milks, K.J. & Straight, A.F., 2010, Dual recognition of CENP-A nucleosomes is required for centromere assembly, *J Cell Biol*, 189(7), pp. 1143-55.

Chen, E.S., Saitoh, S., Yanagida, M. & Takahashi, K., 2003, A cell cycle-regulated GATA factor promotes centromeric localization of CENP-A in fission yeast, *Mol Cell*, 11(1), pp. 175-87.

Chittori, S., Hong, J., Saunders, H., Feng, H., Ghirlando, R., Kelly, A.E., Bai, Y., & Subramaniam, S., 2018 Structural mechanisms of centromeric nucleosome recognition by the kinetochore protein CENP-N. *Science*, 359(6373), pp. 339-43.

Conde e Silva, N., Black, B.E., Sivolob, A., Filipski, J., Cleveland, D.W. & Prunell, A., 2007, CENP-A-containing nucleosomes:easier disassembly versus exclusive centromeric localization, *J Mol Biol*, 370(3), pp. 555-73.

Cooper, J.L. & Henikoff, S., 2004, Adaptive evolution of the histone fold domain in centromeric histones, *Mol Biol Evol*, 21(9), pp. 1712-8.

Dalal, Y., Wang, H., Lindsay, S. & Henikoff, S., 2007, Tetrameric structure of centromeric nucleosomes in interphase Drosophila cells, *PLoS Biol*, 5(8), p. e218.

Dimitriadis, E.K., Weber, C., Gill, R.K., Diekmann, S. & Dalal, Y., 2010, Tetrameric organization of vertebrate centromeric nucleosomes, *Proc Natl Acad Sci U S A*, 107(47), pp. 20317-22.

Díaz-Ingelmo, O., Martínez-García, B., Segura, J., Valdés, A. & Roca, J., 2015, DNA Topology and Global Architecture of Point Centromeres, *Cell Rep*, 13(4), pp. 667-77.

Drinnenberg, I.A., Henikoff, S. & Malik, H.S., 2016, Evolutionary Turnover of Kinetochore Proteins: A Ship of Theseus? *Trends Cell Biol*, 26(7), pp. 498-510.

Earnshaw, W.C. & Rothfield, N., 1985, Identification of a family of human centromere proteins using autoimmune sera from patients with scleroderma, *Chromosoma*, 91(3-4), pp. 313-21.

Falk, S.J., Guo, L.Y., Sekulic, N., Smoak, E.M., Mani, T., Logsdon, G.A., Gupta, K., Jansen, L.E., Van Duyne, G.D., Vinogradov, et al, 2015, Chromosomes. CENP-C reshapes and stabilizes CENP-A nucleosomes at the centromere, *Science*, 348(6235), pp. 699-703.

Falk, S.J., Lee, J., Sekulic, N., Sennett, M.A., Lee, T.H. & Black, B.E., 2016, CENP-C directs a structural transition of CENP-A nucleosomes mainly through sliding of DNA gyres, *Nat Struct Mol Biol*, 23(3), pp. 204-8.

Fang, J., Liu, Y., Wei, Y., Deng, W., Yu, Z., Huang, L., Teng, Y., Yao, T., You, Q., Ruan, H., et al, 2015, Structural transition of centromeric chromatin regulate the cell cycle-dependent recruitment of CENP-N, *Genes Dev*, 29(10):1058-73.

Foltz, D.R., Jansen, L.E., Black, B.E., Bailey, A.O., Yates, J.R.3rd, & Cleveland, D.W., 2006, The human CENP-A centromeric nucleosome-associated complex. *Nat Cell Biol*, 8(5), pp. 458-69.

Fujita, Y., Hayashi, T., Kiyomitsu, T., Toyoda, Y., Kokubu, A., Obuse, C. & Yanagida, M., 2007, Priming of centromere for CENP-A recruitment by human hMis18alpha, hMis18beta, and M18BP1, *Dev Cell*, 12(1), pp. 17-30.

Fukagawa, T., Pendon, C., Morris, J. & Brown, W., 1999, CENP-C is necessary but not sufficient to induce formation of a functional centromere, *The EMBO journal*, 18(15), pp. 4196-209.

Furuyama, T. & Henikoff, S., 2009, Centromeric nucleosomes induce positive DNA supercoils, *Cell*, 138(1), pp. 104-13.

Furuyama, T., Codomo, C.A. & Henikoff, S., 2013, Reconstitution of hemisomes on budding yeast centromeric DNA, *Nucleic acids research*, 41(11), pp. 5769-83.

Gonen, S., Akiyoshi, B., Iadanza, M.G., Shi, D., Duggan, N., Biggins, S. & Gonen, T., 2012, The structure of purified kinetochores reveals multiple microtubule-attachment sites, *Nat Struct Mol Biol*, 19(9), pp. 925-9.

Guo, L.Y., Allu, P.K., Zandarashvili, L., McKinley, K.L., Sekulic, N., Dawicki-McKenna, J.M., Fachinetti, D., Logsdon, G.A., Jamiolkowski, R.M., Cleveland, D.W., et al, 2017, Centromeres are maintained by fastening CENP-A to DNA and directing an arginine anchor-dependent nucleosome transition, *Nat Commun*, 8, p. 15775.

Heinz, W.F., & Hoh, J.H., Spatially resolved force spectroscopy of biological surfaces using the atomic force microscope. *Trends Biotechnol.* 17(4):143-50 .

Henikoff, S., Ahmad, K. & Malik, H.S., 2001, The centromere paradox: stable inheritance with rapidly evolving DNA, *Science*, 293(5532), pp. 1098-102.

Howman, E.V., Fowler, K.J., Newson, A.J., Redward, S., MacDonald, A.C., Kalitsis, P. & Choo, K.H., 2000, Early disruption of centromeric chromatin organization in centromere protein A (Cenpa) null mice, *Proc Natl Acad Sci U S A*, 97(3), pp. 1148-53.

Kalitsis, P., Fowler, K.J., Earle, E., Hill, J. & Choo, K.H., 1998, Targeted disruption of mouse centromere protein C gene leads to mitotic disarray and early embryo death, *Proc Natl Acad Sci U S A*, 95(3), pp. 1136-41.

Kato, H., Jiang, J., Zhou, B.R., Rozendaal, M., Feng, H., Ghirlando, R., Xiao, T.S., Straight, A.F. & Bai, Y., 2013, A conserved mechanism for centromeric nucleosome recognition by centromere protein CENP-C, *Science*, 340(6136), pp. 1110-3.

Kim, S.H., Vlijm, R., van der Torre, J., Dalal, Y. & Dekker, C., 2016, CENP-A and H3 Nucleosomes Display a Similar Stability to Force-Mediated Disassembly, *PLoS One*, 11(11), p. e0165078.

Kono, H., Shirayama, K., Arimura, Y., Tachiwana, H. & Kurumizaka, H., 2015, Two arginine residues suppress the flexibility of nucleosomal DNA in the canonical nucleosome core, *PLoS One*, 10(3), p. e0120635.

Kwon, M.S., Hori, T., Okada, M. & Fukagawa, T., 2007, CENP-C is involved in chromosome segregation, mitotic checkpoint function, and kinetochore assembly, *Mol Biol Cell*, 18(6), pp. 2155-68.

Lacoste, N., Woolfe, A., Tachiwana, H., Garea, A.V., Barth, T., Cantaloube, S., Kurumizaka, H., Imhof, A. & Almouzni, G., 2014, Mislocalization of the centromeric histone variant CenH3/CENP-A in human cells depends on the chaperone DAXX, *Mol Cell*, 53(4), pp. 631-44.

Maheshwari, S., Tan, E.H., West, A., Franklin, F.C., Comai, L. & Chan, S.W., 2015, Naturally occurring differences in CENH3 affect chromosome segregation in zygotic mitosis of hybrids, *PLoS Genet*, 11(1), p. e1004970.

Malik, H.S. & Henikoff, S., 2001, Adaptive evolution of Cid, a centromere-specific histone in Drosophila, *Genetics*, 157(3), pp. 1293-8.

McKinley, K.L. & Cheeseman, I.M., 2016, The molecular basis for centromere identity and function, *Nat Rev Mol Cell Biol*, 17(1), pp. 16-29.

Melters, D.P., Bradnam, K.R., Young, H.A., Telis, N., May, M.R., Ruby, J.G., Sebra, R., Peluso, P., Eid, J., Rank, D., et al, 2013, Comparative analysis of tandem repeats from hundreds of species reveals unique insights into centromere evolution, *Genome Biol*, 14(1), p. R10.

Mendiburo, M.J., Padeken, J., Fülöp, S., Schepers, A. & Heun, P., 2011, Drosophila CENH3 is sufficient for centromere formation, *Science*, 334(6056), pp. 686-90.

Meraldi, P., McAinsh, A.D., Rheinbay, E. & Sorger, P.K., 2006, Phylogenetic and structural analysis of centromeric DNA and kinetochore proteins, *Genome Biol*, 7(3), p. R23.

Moroi, Y., Peebles, C., Fritzler, M.J., Steigerwald, J. & Tan, E.M., 1980, Autoantibody to centromere (kinetochore) in scleroderma sera, *Proc Natl Acad Sci U S A*, 77(3), pp. 1627-31.

Müller, S., & Almouzni, G., 2017, Chromatin dynamics during the cell cycle at centromeres, *Nat Rev Genet*, 18(3):192-206.

Noll, M., 1974, Internal structure of the chromatin subunit, *Nucleic acids research*, 1(11), pp. 1573-8.

Palmer, D.K., O'Day, K., Trong, H.L., Charbonneau, H. & Margolis, R.L., 1991, Purification of the centromere-specific protein CENP-A and demonstration that it is a distinctive histone, *Proc Natl Acad Sci U S A*, 88(9), pp. 3734-8.

Panchenko, T., Sorensen, T.C., Woodcock, C.L., Kan, Z.Y., Wood, S., Resch, M.G., Luger, K., Englander, S.W., Hansen, J.C., & Black, B.E., 2011, Replacement of histone H3 with CENP-A directs global nucleosome array condensation and loosening of nucleosome superhelical termini, *Proc Natl Acad Sci U S A*, 108(40), pp. 16588-93.

Pentakota, S. Zhou, K., Smith, C., Miffini, S., Petrovic, A., Morgan, G.P., Weir, J.R., Vetter, I.R., Musacchio, A., & Luger, K., 2018 Deconding the centromeric nucleosome through CENP-N. *eLife*, e33442.

Pesenti, M.E., Weir, J.R. & Musacchio, A., 2016, Progress in the structural and functional characterization of kinetochores, *Curr Opin Struct Biol*, 37, pp. 152-63.

Polach, K.J. & Widom, J., 1995, Mechanism of protein access to specific DNA sequences in chromatin: a dynamic equilibrium model for gene regulation, *J Mol Biol*, 254(2), pp. 130-49.

Rakshit, T., Banerjee, S., Mishra, S., Mukhopadhyay, R., 2013, Nanoscale mechano-electronic behavior of a metalloprotein as a variable of metal content. *Langmuir*, 29(40):12511-9.

Régnier, V., Vagnarelli, P., Fukagawa, T., Zerjal, T., Burns, E., Trouche, D., Earnshaw, W. & Brown, W., 2005, CENP-A is required for accurate chromosome segregation and sustained kinetochore association of BubR1, *Mol Cell Biol*, 25(10), pp. 3967-81.

Ross, B.D., Rosin, L., Thomae, A.W., Hiatt, M.A., Vermaak, D., de la Cruz, A.F., Imhof, A., Mellone, B.G. & Malik, H.S., 2013, Stepwise evolution of essential centromere function in a Drosophila neogene, *Science*, 340(6137), pp. 1211-4.

Roulland, Y., Ouararhni, K., Naidenov, M., Ramos, L., Shuaib, M., Syed, S.H., Lone, I.N., Boopathi, R., Fontaine, E., Papai, G., et al, 2016, The Flexible Ends of CENP-A Nucleosome Are Required for Mitotic Fidelity, *Mol Cell*, 63(4), pp. 674-85.

Rudd, M.K., Wray, G.A. & Willard, H.F., 2006, The evolutionary dynamics of alpha-satellite, *Genome research*, 16(1), pp. 88-96.

Sekulic, N., Bassett, E.A., Rogers, D.J., & Black, B.E., 2010, The structure of (CENP-A-H4)(2) reveals physical features that mark centromeres. *Nature*, 467(7313):347-51.

Smoak, E.M., Stein, P., Schultz, R.M., Lampson, M.A. & Black, B.E., 2016, Long-Term Retention of CENP-A Nucleosomes in Mammalian Oocytes Underpins Transgenerational Inheritance of Centromere Identity, *Curr Biol*, 26(8), pp. 1110-6.

Stumme-Diers, M.P., Banerjee, S., Hashemi, M., Sun, Z., & Lyubchenko, Y.L., 2018, Nanoscale dynamics of centromere nucleosomes and the critical roles of CENP-A. *Nucleic Acid Res*, 46(1):94-103.

Suzuki, A., Badger, B.L. & Salmon, E.D., 2015, A quantitative description of Ndc80 complex linkage to human kinetochores, *Nat Commun*, 6, p. 8161.

Suzuki, A., Hori, T., Nishino, T., Usukura, J., Miyagi, A., Morikawa, K. & Fukagawa, T., 2011, Spindle microtubules generate tension-dependent changes in the distribution of inner kinetochore proteins, *J Cell Biol*, 193(1), pp. 125-40.

Tachiwana, H., Kagawa, W., Shiga, T., Osakabe, A., Miya, Y., Saito, K., Hayashi-Takanaka, Y., Oda, T., Sato, M., Park, et al, 2011, Crystal structure of the human centromeric nucleosome containing CENP-A, *Nature*, 476(7359), pp. 232-5.

Talbert, P.B., Bryson, T.D. & Henikoff, S., 2004, Adaptive evolution of centromere proteins in plants and animals, *J Biol*, 3(4), p. 18.

van Hooff, J.J., Tromer, E., van Wijk, L.M., Snel, B. & Kops, G.J., 2017, Evolutionary dynamics of the kinetochore network in eukaryotes as revealed by comparative genomics, *EMBO Rep*.

Vlijm, R., Kim, S.H., De Zwart, P.L., Dalal, Y. & Dekker, C., 2017, The supercoiling state of DNA determines the handedness of both H3 and CENP-A nucleosomes, *Nanoscale*, 9(5), pp. 1862-70.

Vinckier, A., & Semenza, G., 1998, Measuring elasticity of biological materials by atomic force miscroscopy. *FEBS Lett*, 430, pp. 12-6.

Walkiewicz, M. P., Dimitriadis, E. K. & Dalal, Y., 2014, CENP-A octamers do not confer a reduction in nucleosome height by AFM, *Nat Struct Mol Biol,* 21, pp. 2-3

Widom, J., 1998, Structure, dynamics, and function of chromatin in vitro, *Annu Rev Biophys Biomol Struct*, 27, pp. 285-327.

Williams, J.S., Hayashi, T., Yanagida, M. & Russell, P., 2009, Fission yeast Scm3 mediates stable assembly of Cnp1/CENP-A into centromeric chromatin, *Mol Cell*, 33(3), pp. 287-98.

Winogradoff, D., Zhao, H., Dalal, Y. & Papoian, G.A., 2015, Shearing of the CENP-A dimerization interface mediates plasticity in the octameric centromeric nucleosome, *Sci Rep*, 5, p. 17038.

Wisniewski, J., Hajj, B., Chen, J., Mizuguchi, G., Xiao, H., Wei, D., Dahan, M. & Wu, C., 2014, Imaging the fate of histone Cse4 reveals de novo replacement in S phase and subsequent stable residence at centromeres, *Elife*, 3, p. e02203.

Figure legends

Figure 1. CENP-A nucleosomes are elastic, but rigidifies upon CENP-C^{CD} binding

(A) The free energy landscape of CENP-A nucleosomes alone or CENP-A nucleosome with CENP-C^{CD} fragment was determined by principle component analysis. CENP-A nucleosomes display a rugged free energy landscape, which is locked down when CENP-C^{CD} is bound, increasing the connectivity of the energetic minima. (B) To be able to determine the Young's modulus of CENP-A and H3 nucleosome arrays, we *in vitro* reconstituted these arrays by salt dialysis. (C) Representative AFM images and force curves with Hertz model (spherical indenter) of reconstituted H3, CENP-A nucleosomes, and CENP-A nucleosomes incubated in the presence of the CENP-C^{CD} fragment are shown. (D) Histogram of Young's modulus values showing that CENP-A nucleosomes are more elastic than H3 nucleosomes. Upon binding with the CENP-C^{CD} CENP-A nucleosomes became rigidified (ANOVA test $P<0.0001$). (E)Tabular and graphical representation of the Young's modulus for H3, CENP-A, CENP-A nucleosomes with CENP-C^{CD}.

Figure 2. Two distinct classes of CENP-A nucleosome are found at centromere

(A) Extracted chromatin was separated by a 5-20% glycerol gradient sedimentation assay from which twelve fractions were isolated. (B) DNA per fraction was isolated and separated on a 1.2% agarose gel. (C) Histone content per fraction was determined by SDS-PAGE. (D) First, CENP-C

N-ChIP was performed on each fraction and ran on a SDS-PAGE gels, which was probed for CENP-C and CENP-A. (E) Second, serial ACA N-ChIP was performed on all fraction of the unbound chromatin from the CENP-C N-ChIP and ran on a SDS-PAGE and probed for CENP-C and CENP-A. All experiments were performed in triplicates. (F) Quantification of relative CENP-A contribution per fraction as shown in C-E.

Figure 3. CENP-C binds to small subset of CENP-A nucleosomes

(A) To determine what the relative amount of CENP-A that is bound to CENP-C in randomly cycling HeLa cells, we performed a serial N-ChIP on 6-minute digested chromatin. (B) Western blot analysis of the serial N-ChIP was performed and probed for H2A, H3, CENP-A, and CENP-C. (C) Quantification of eleven independent experiments revealed that a 6-fold difference between CENP-A bound to CENP-C. (C) Probing for γH2A.X, H2A.Z, and macroH2A. (C) Quantification of four independent experiments revealed that none of the H2A variants was enriched in either CENP-A population. As a control, we measured the relative amount of H2B over H4.

Figure 4. Inner kinetochore associated nucleosomes are not enriched for histone H2A variants, and bulk CENP-A nucleosomes wrap DNA loosely

(A) To determine whether CENP-C N-ChIP brings down inner kinetochore components, we performed western blot analysis. On the other hand, to determine how DNA is wrapped around nucleosomes, we isolated predominantly mononucleosomes following 15 minute MNase digestion of nuclei. Next, we performed serial N-ChIP to purify CENP-C associated chromatin and CENP-A nucleosomes. (B) Cartoon representation of inner kinetochore composition. (C)

Western blot analysis of three independent experiments showing that inner kinetochore components. (D) Samples were digested with DNase I digestion and subsequently DNA was extracted and ran on a high resolution 10% TBE with urea gel. (E) A density plot of high resolution urea TBE gel. All experiments were performed in triplicates.

Figure 5. Immuno-AFM confirms CENP-C associates with CENP-A nucleosomes

(A) To confirm that CENP-C associated with CENP-A nucleosomes particles, we performed immune-AFM on *in vitro* reconstituting H3 and CENP-A nucleosomes in parallel to extracted bulk and CENP-C associated chromatin. (B) Representative images for three conditions per sample, including a blank control. The scale bar is 30 nm. (C) Height measurement of all three conditions were plotted per sample, showing that anti-CENP-A antibody only recognized *in vitro* reconstituted CENP-A nucleosomes and nucleosomes associated with CENP-C.

Figure 6. CENP-A nucleosomes associated with the inner kinetochore are octameric in height

(A) Chromatin was extracted from HeLa cells after 6-minute digestion, followed by either mock, CENP-A, or CENP-C N-ChIP. Unbound chromatin was used as bulk chromatin. (B) Representative AFM and (C) TEM images of either mock, bulk chromatin, CENP-A chromatin, or CENP-C chromatin. The scale bar is 50 nm. (D) Nucleosomal heights was determined for all three AFM samples. The mean height with standard deviations are shown, as well as their distribution. (E) Based on AFM and TEM images, a model emerges where several CENP-A nucleosomes are in close proximity to the CENP-C complex/inner kinetochore, including a stretch of ~230-bp of naked DNA that is refractory to MNase digestion.

Figure 7. Rigidified CENP-A chromatin interferes with RNAP2 recruitment

(A) Schematic representation how HeLa cells were synchronized to late M/early G1 by double thymidine block. (B) All-atom computational modeling of DNA gyre gapping or DNA gyre sliding of CENP-A nucleosome alone or bound to either 1 or 2 CENP-C^{CD} fragments. (C) In-fluid, single-molecule, nano-indentation force spectroscopy AFM of CENP-A nucleosome arrays in the absence or presence of 2.2X or 4X CENP-C^{CD} fragment. (D) Chromatin compaction was measured by average circumference of particles, as this would distinguish both compacted chromatin and clustered nucleosomes from individual nucleosomes. *In vitro* reconstituted CENP-A nucleosomes with and without CENP-C^{CD}, and *in vivo* ACA N-ChIP samples with and without either the addition of CENP-C^{CD} or CENP-C OE were compared. (* < 0.05; ** < 0.005) (E) Western blot analysis of serial N-ChIP probing for RNAP2 and various centromere and chromatin markers. Quantification of RNAP2 and CENP-A levels were determined. (F) *De novo* CENP-A incorporation was assessed by quench pulse-chase immunofluorescence. After old CENP-A was quenched with TMR-block, newly loaded CENP-A was stained with TMR-Star and foci intensity was measured over total CENP-A foci intensity. (** < 0.005). (G) Model how a balance between flexible and rigidified CENP-A nucleosomes govern accessibility of centromeric chromatin of RNAP2 and *de novo* incorporation of CENP-A.

Figure 1

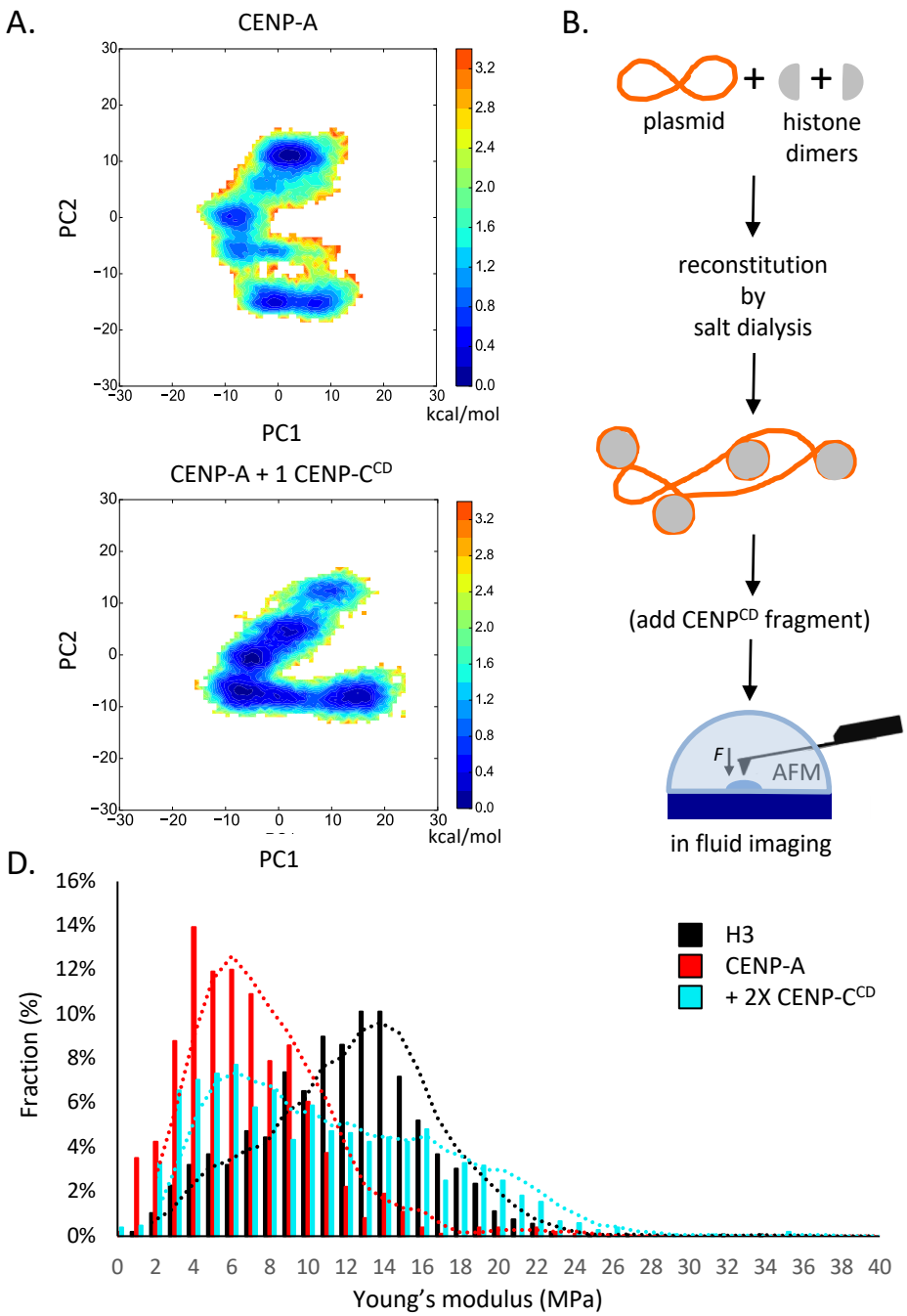

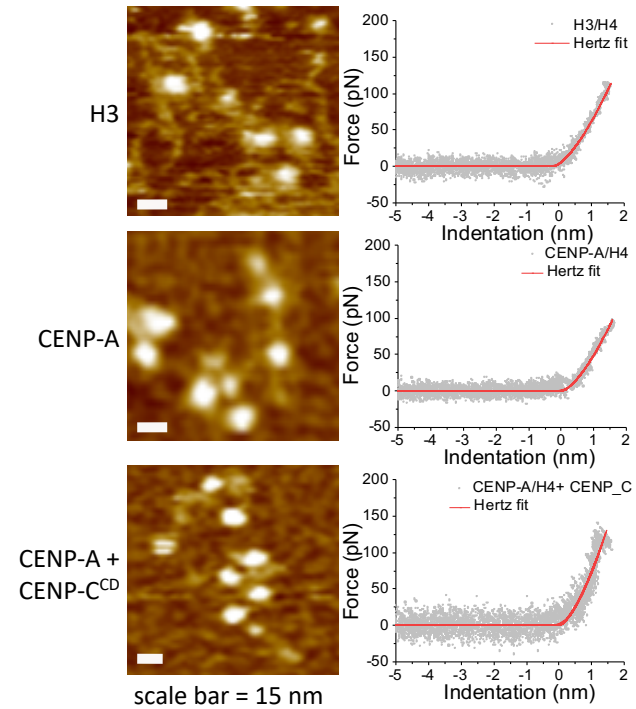

E.

Nucleosome	Young's modulus (MPa)	Height (nm)
H3	11.1±4.5	3.81±0.31
CENP-A	6.4±3.9	3.74±0.29
CENP-A + 2X CENP-C^CD	10.0±5.9	4.12±0.44

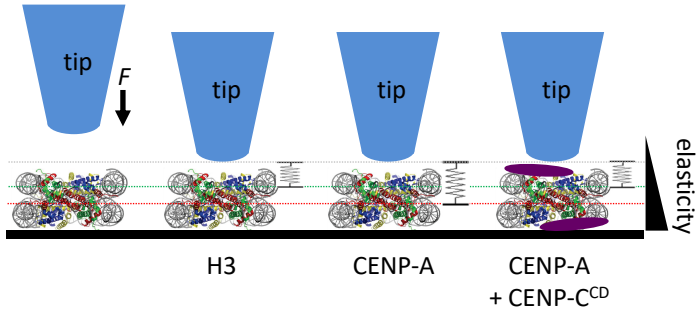

Figure 2

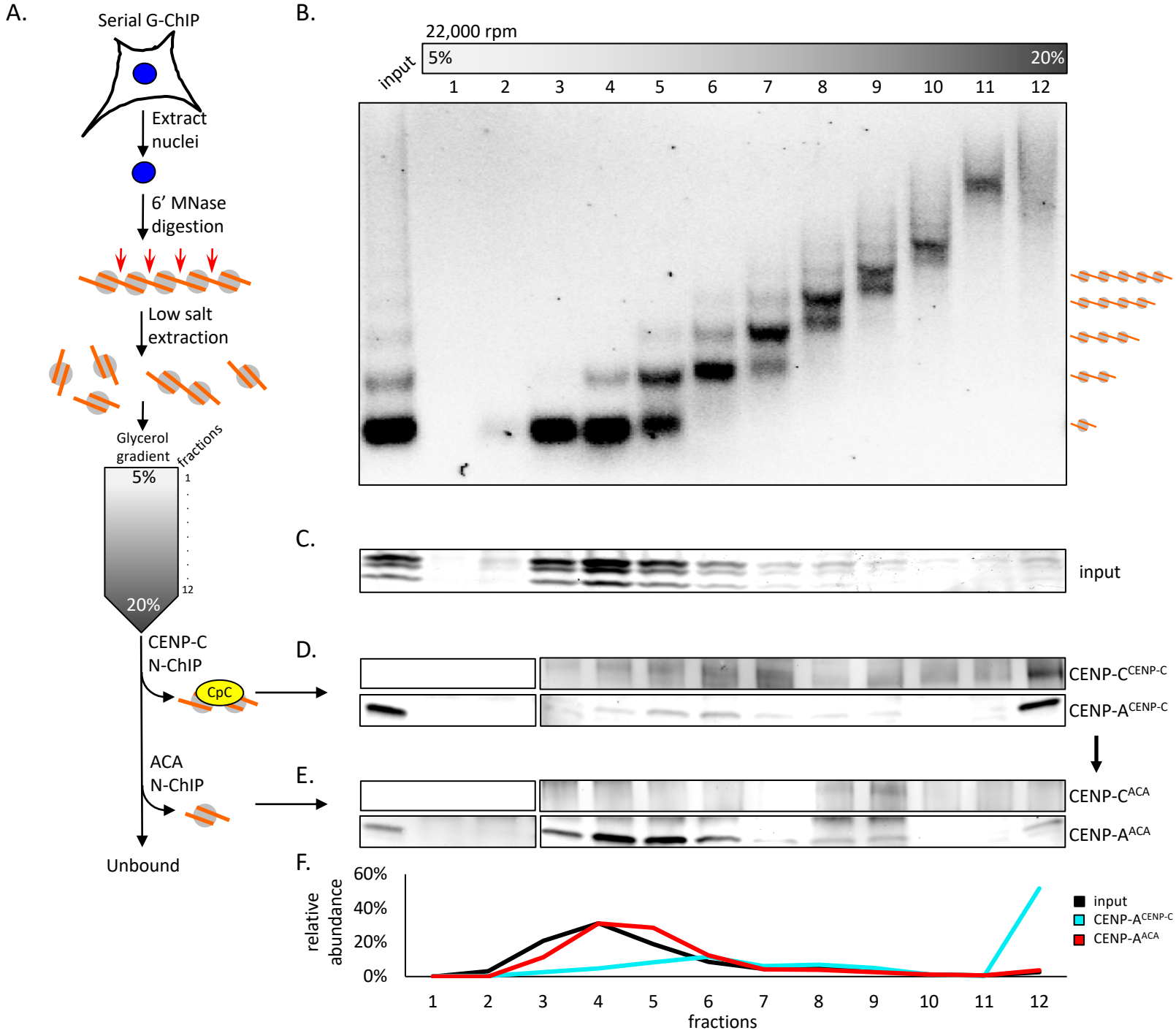
A.
Serial G-ChIP
Extract nuclei
6' MNase digestion
Low salt extraction
Glycerol gradient
fractions
5%
20%
1
12
CENP-C N-ChIP
CpC
ACA N-ChIP
Unbound
B.
22,000 rpm
input
5%
20%
1 2 3 4 5 6 7 8 9 10 11 12
C.
input
D.
CENP-C^CENP-C
CENP-A^CENP-C
E.
CENP-C^ACA
CENP-A^ACA
F.
relative abundance
60%
40%
20%
0%
1 2 3 4 5 6 7 8 9 10 11 12
fractions
input
CENP-A^CENP-C
CENP-A^ACA

Figure 3

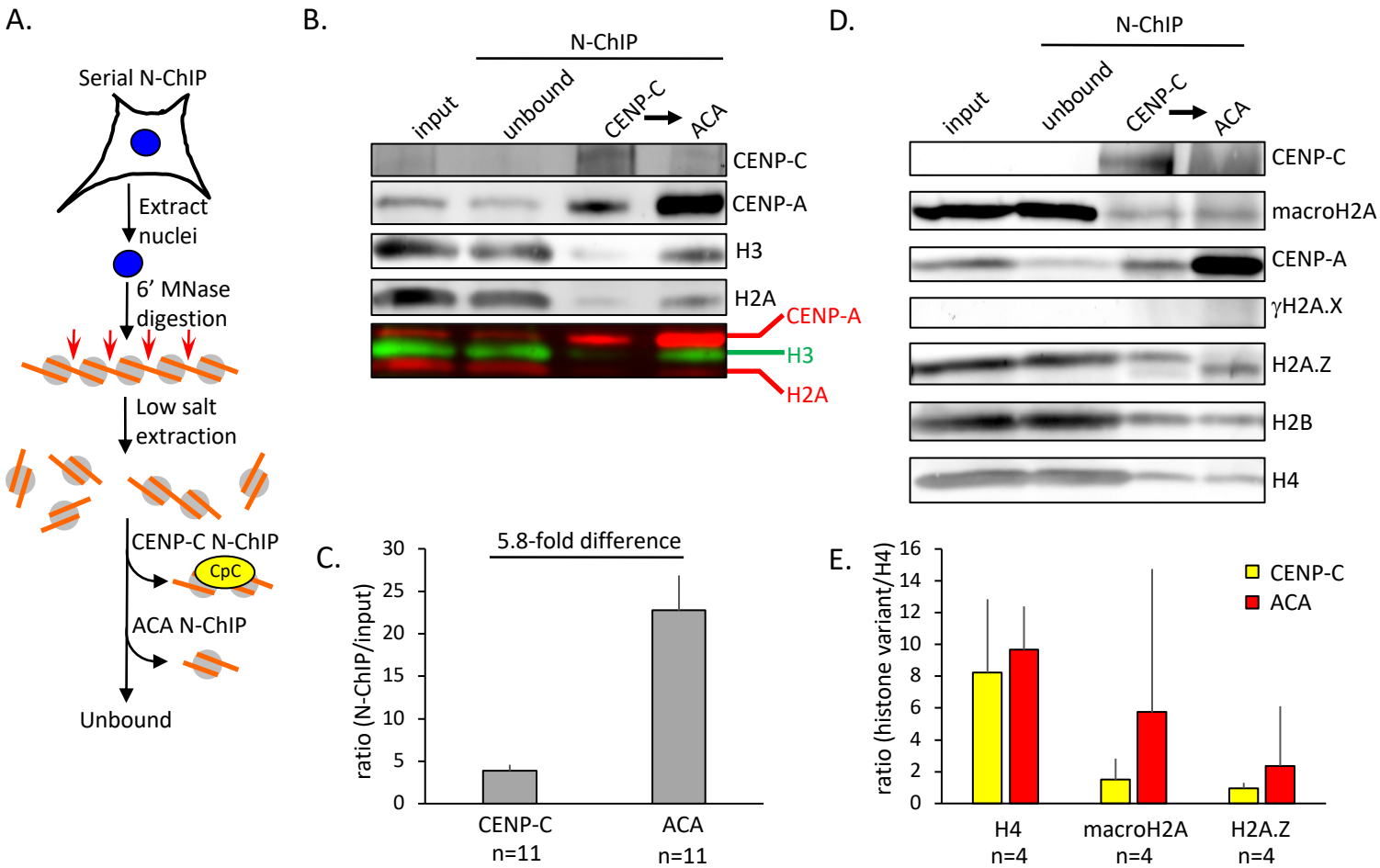
A.
Serial N-ChIP
Extract nuclei
6' MNase digestion
Low salt extraction
CENP-C N-ChIP
CpC
ACA N-ChIP
Unbound
B.
N-ChIP
input
unbound
CENP-C
ACA
CENP-C
CENP-A
H3
H2A
CENP-A
H3
H2A
D.
N-ChIP
input
unbound
CENP-C
ACA
CENP-C
macroH2A
CENP-A
γH2A.X
H2A.Z
H2B
H4
C.
5.8-fold difference
ratio (N-ChIP/input)
30
25
20
15
10
5
0
CENP-C
n=11
ACA
n=11
E.
ratio (histone variant/H4)
16
14
12
10
8
6
4
2
0
CENP-C
ACA
H4
n=4
macroH2A
n=4
H2A.Z
n=4

Figure 4

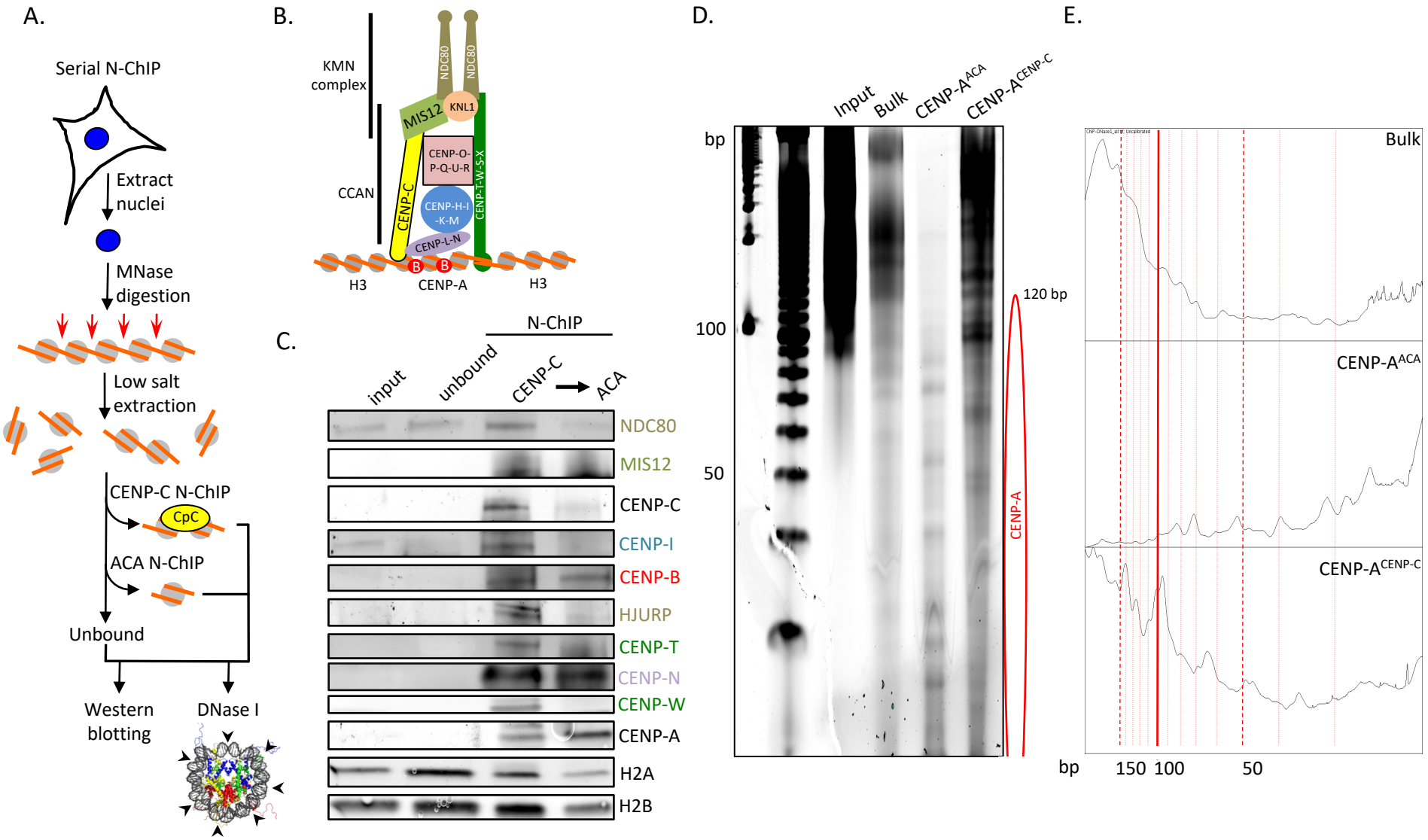
A.
Serial N-ChIP
Extract nuclei
MNase digestion
Low salt extraction
CENP-C N-ChIP
CpC
ACA N-ChIP
Unbound
Western blotting
DNase I
B.
KMN complex
CCAN
NDC80
NDC80
MIS12
KNL1
CENP-O-P-Q-U-R
CENP-C
CENP-T-W-S-X
CENP-H-I-K-M
CENP-L-N
B
B
H3
CENP-A
H3
C.
N-ChIP
input
unbound
CENP-C
ACA
NDC80
MIS12
CENP-C
CENP-I
CENP-B
HJURP
CENP-T
CENP-N
CENP-W
CENP-A
H2A
H2B
D.
Input
Bulk
CENP-A^ACA
CENP-A^CENP-C
bp
100
50
120 bp
CENP-A
E.
Bulk
CENP-A^ACA
CENP-A^CENP-C
bp
150
100
50

Figure 5

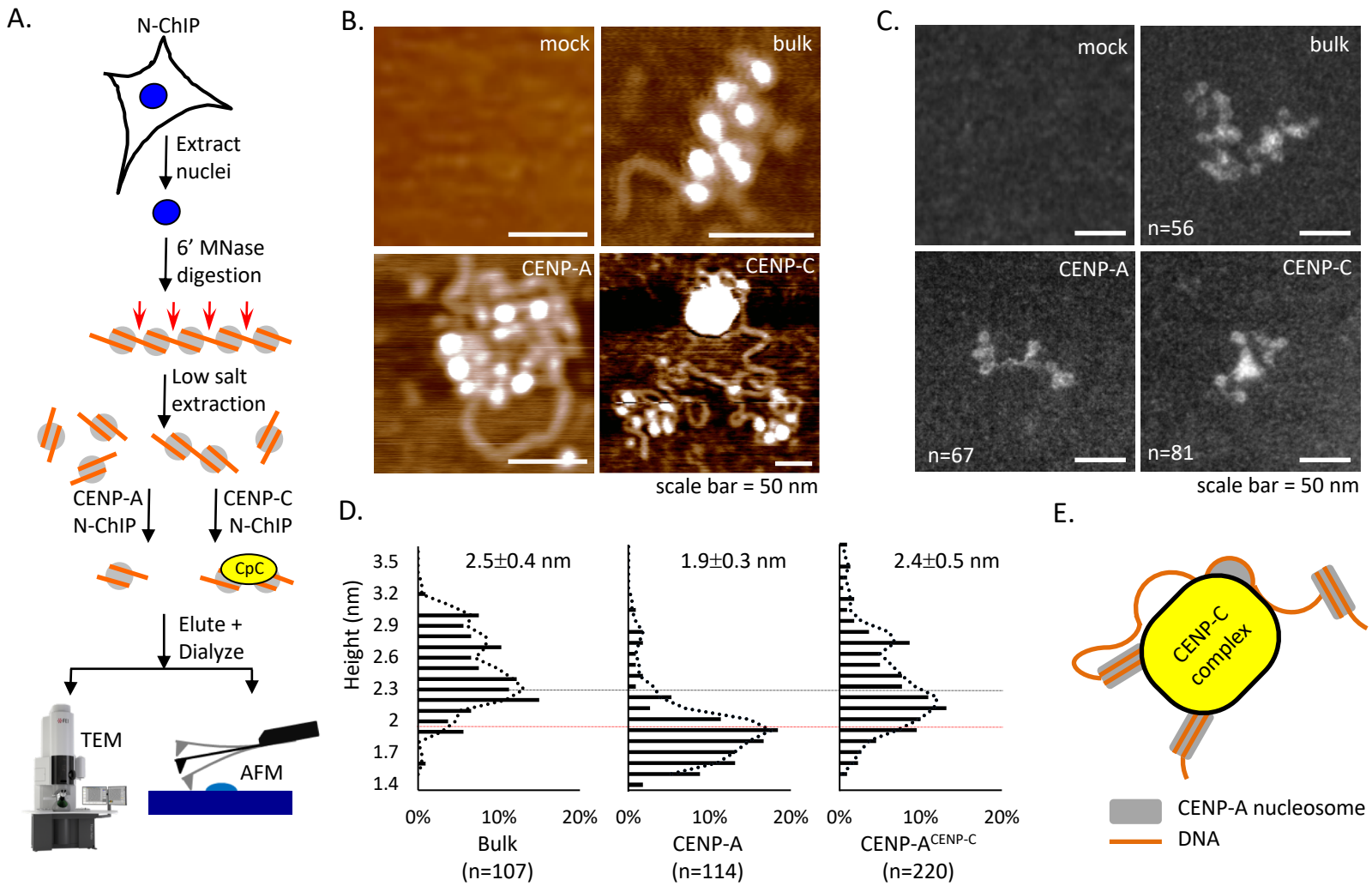
A.
N-ChIP
Extract nuclei
6' MNase digestion
Low salt extraction
CENP-A N-ChIP
CENP-C N-ChIP
CpC
Elute + Dialyze
TEM
AFM
B.
mock
bulk
CENP-A
CENP-C
scale bar = 50 nm
C.
mock
bulk
n=56
CENP-A
CENP-C
n=67
n=81
scale bar = 50 nm
D.
Height (nm)
3.5
3.2
2.9
2.6
2.3
2
1.7
1.4
2.5±0.4 nm
1.9±0.3 nm
2.4±0.5 nm
0%
10%
20%
Bulk (n=107)
CENP-A (n=114)
CENP-A^CENP-C (n=220)
E.
CENP-C complex
CENP-A nucleosome
DNA

Figure 6

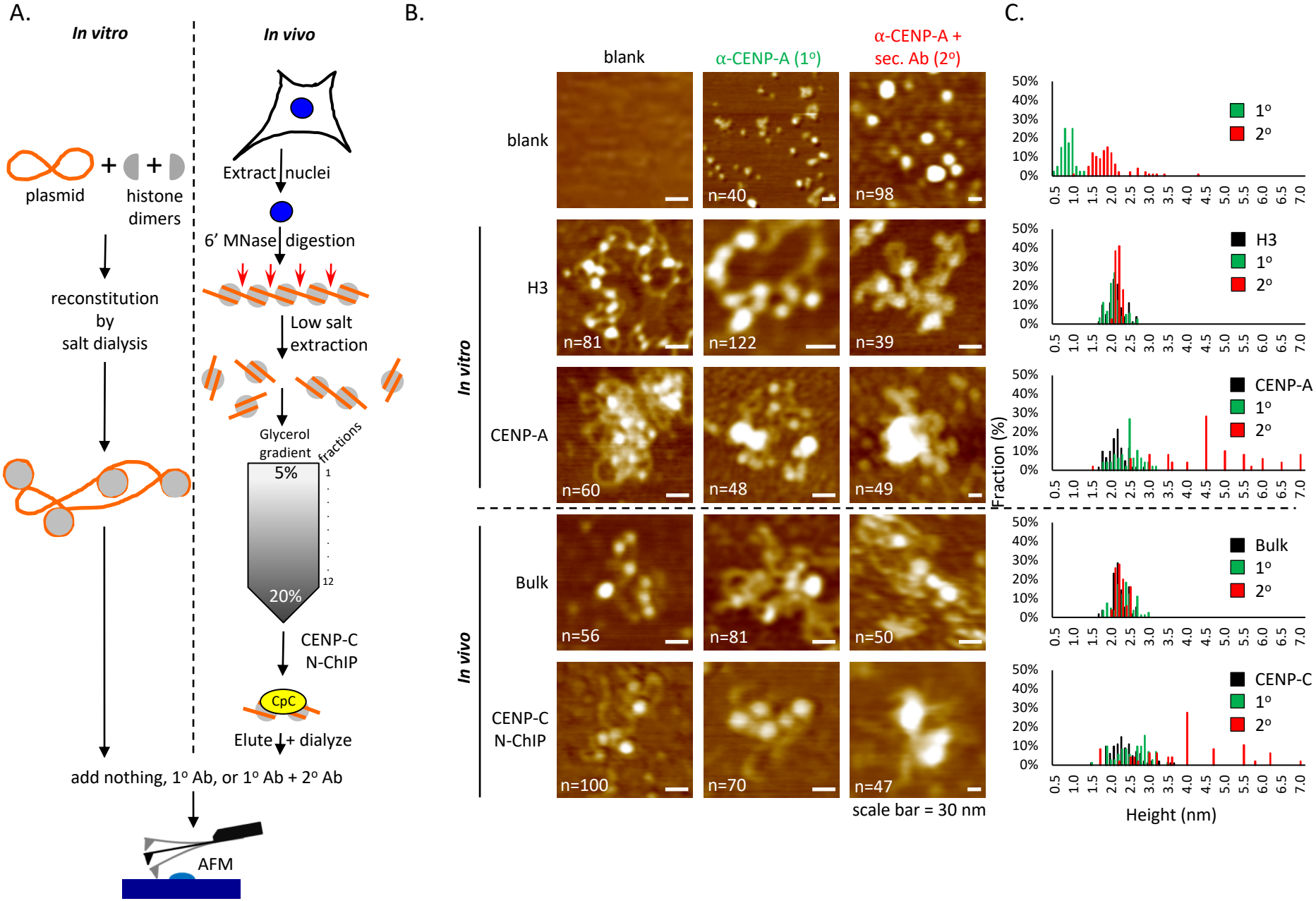
A.
In vitro
In vivo
plasmid
histone dimers
reconstitution by salt dialysis
Extract nuclei
6' MNase digestion
Low salt extraction
Glycerol gradient
fractions
5%
20%
1
12
CENP-C N-ChIP
CpC
Elute + dialyze
add nothing, 1° Ab, or 1° Ab + 2° Ab
AFM
B.
blank
α-CENP-A (1°)
α-CENP-A + sec. Ab (2°)
blank
H3
CENP-A
Bulk
CENP-C N-ChIP
In vitro
In vivo
n=40
n=98
n=81
n=122
n=39
n=60
n=48
n=49
n=56
n=81
n=50
n=100
n=70
n=47
scale bar = 30 nm
C.
Fraction (%)
Height (nm)
1°
2°
H3
CENP-A
Bulk
CENP-C

Figure 7

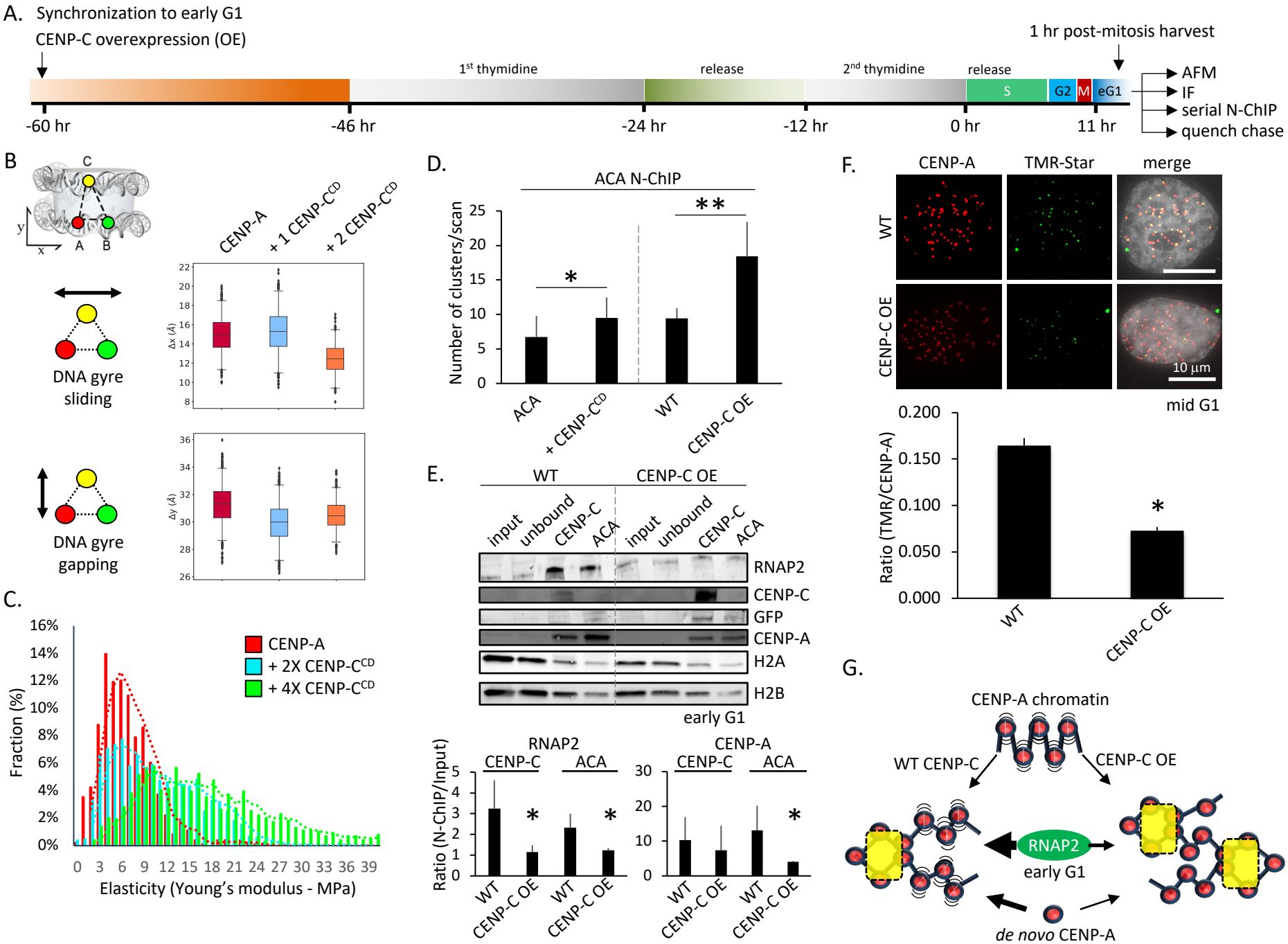
A.
Synchronization to early G1
CENP-C overexpression (OE)
1st thymidine
release
2nd thymidine
release
S
G2
M
eG1
1 hr post-mitosis harvest
AFM
IF
serial N-ChIP
quench chase
-60 hr
-46 hr
-24 hr
-12 hr
0 hr
11 hr
B
C
A
B
y
x
CENP-A
+ 1 CENP-C^CD
+ 2 CENP-C^CD
DNA gyre sliding
DNA gyre gapping
Δx (Å)
Δy (Å)
C.
CENP-A
+ 2X CENP-C^CD
+ 4X CENP-C^CD
Fraction (%)
Elasticity (Young's modulus - MPa)
D.
ACA N-ChIP
Number of clusters/scan
ACA
+ CENP-C^CD
WT
CENP-C OE
E.
WT
CENP-C OE
input
unbound
CENP-C
ACA
RNAP2
CENP-C
GFP
CENP-A
H2A
H2B
early G1
RNAP2
CENP-A
Ratio (N-ChIP/Input)
F.
CENP-A
TMR-Star
merge
WT
CENP-C OE
10 µm
mid G1
Ratio (TMR/CENP-A)
G.
CENP-A chromatin
WT CENP-C
CENP-C OE
RNAP2
early G1
de novo CENP-A

STAR Methods

Key Resources Table

Reagents or Resource	**Source**	**Identifier**
Antibodies		
ACA serum	BBI Solutions	SG140-2
Anti-GFP	Santa Cruz	sc-9996
Anti-CENP-A (mouse)	Abcam	ab13939
Anti-CENP-A (rabbit)	Abcam	ab45694
Anti-CENP-A (rabbit)	Milipore	04-205
Anti-CENP-B (rabbit)	Santa Cruz	sc-22788
Anti-CENP-C (guinea pig)	MBL International	PD030
Anti-CENP-C (rabbit)	Santa Cruz	sc-22789
Anti-RNA polymerase II	Millipore	05-623
Anti-RNA polymerase II	Abcam	ab5095
Anti-CENP-N	Avivasysbio	ARP57258-P050
Anti-CENP-I	Bethyl	A303-374A
Anti-CENP-T	Bethyl	A302-314A
Anti-CENP-W	Invitrogen	PA5-34441
Anti-MIS12	Abcam	ab70843
Anti-HEC1/NDC80	GeneTex	GTX70268
Anti-macroH2A.1	Abcam	ab37264
Anti-γH2A.X	Abcam	ab2893
Anti-γH2A.X	Abcam	ab11174
Anti-H2A.Z	Abcam	ab4179
Anti-H2A	Abcam	ab18255
Anti-H2B	Abcam	ab1790
Anti-H4	Cell Signaling	2935T
Anti-H3	Santa Cruz	sc-8654
Software and Algorithms		
RepBase		hhtp://www.girinst.org/repbase
Gwyddion		http://gwyddion.net/
R		https://www.r-project.org/
NIH ImageJ		https://imagej.nih.gov/ij/
Bio-Formats		https://www.openmicroscopy.org/bio-formats/
PyMOL		https://pymol.org/2/
CRaQ		http://facilities.igc.gulbenkian.pt/microscopy/microscopy-macros.php

Contact for Reagent and Resource Sharing
Requests for further information or reagents should be directed to the Lead Contact, Yamini Dalal (dalaly@mail.nih.gov)

Experimental Model and Subject Detail
HeLa cells (female cells derived from cervical adenocarcinoma) were obtained from ATCC CCL-2 and grown at 37ºC and 5% CO2 in T-175 tissue culture flasks from Sarstedt (Cat. #83.3912.002).

Methods Details
All-atom computational modeling
Two nucleosomal systems were built for simulation: the CENP-A nucleosome as described previously (Bui et al 2017) and the CENP-A nucleosome with CENP-C fragment bound from PDB ID: 4X23 (Kato et al 2013). The CENP-C^{CD} fragments were docked onto the CENP-A interface using the CE algorithm (Shindyalov & Bourne 1998) of PyMOL (The PyMol Molecular Graphics System). Both systems were started from the final time point of our previous 1 µs simulation and the coordinates, velocities, parameters, and system setup and analysis methods were replicated (Bui et al 2017). Both CENP-A and CENP-A with one and two CENP-C^{CD} bound were simulated for an additional microsecond and the first 600 ns of simulation time were truncated from the dataset for further analysis and to account for equilibration. Furthermore, we calculated the relative positions of three phosphate backbone atoms at positions -33, -43, and +38 numbered from the 5' (−) to 3' (+) direction relative to the pseudo-dyad. The distances between these points and the skew of the triangle formed were measured and then plotted with the initial position of residue -33 set to (0,0) on an xy-plane. The distribution of Δy and Δx of +38 relative to -33 and -34 was used to measure DNA gaping and sliding respectively. These distributions were visualized with standard box plots showing the mean, the central rectangle showing the interquartile range, and whiskers extending to the extrema. The distribution of polygons contains the minima and mxima of all three vertices were plotted visually with triangles to visually represent changes in skew and the range of sizes.

Native Chromatin-Immunoprecipitation and western blotting
Human cell line HeLa were grown in DMEM (Invitrogen/ThermoFisher Cat #11965) supplemented with 10% FBS and 1X penicillin and streptomycin cocktail. N-ChIP experiments were performed without fixation. After cells were grown to ~80% confluency, they were harvested as described here (Bui et al 2012; Bui et al 2017), but with a few modifications. In short, cells were harvested, washed with PBS and PBS containing 0.1% Tween 20 (Sigma-Aldrich cat #P7949). Nuclei were released with TM2 (20 mM Tris-HCl, pH 8.0; 2 mM $MgCl_2$; 0.5 mM PMSF) with 0.5% Nonidet P-40 (Sigma-Aldrich cat #74385). Afterwards, nuclei were washed with TM2 and dissolved in a total volume of 2 mL of 0.1 M TE (10 mM Tris-HCl, pH 8.0; 0.2 mM EDTA, 100 mM NaCl). Subsequently, chromatin was digested for 6 minutes with 0.25 U MNase (Sigma-Aldrich cat #N3755-500UN) and supplemented with 1.5 mM $CaCl_2$. MNase reaction was quenched with 10 mM EGTA. All centrifugations were done at 1000 rpm at 4ºC. The cell or nuclei pellet was only tapped once to facilitate braking them up. Supernatant was removed, and chromatin extracted overnight in low salt solution (0.5X PBS; 0.1 mM EGTA supplemented with a protease inhibitor cocktail (Roche cat #05056489001). N-ChIP chromatin bound to Protein G Sepharose beads (GE Healthcare cat #17-0618-02) were washed twice with ice cold 0.5X PBS and spun down for 1 minute at 4ºC at 800 rpm. For a serial N-ChIP, the first unbound fraction was saved and subjected to a second N-ChIP. Westerns were done using LiCor's Odyssey CLx scanner and Image Studio v2.0.
For CENP-C overexpression we transfected HeLa cells with pEGFP-CENP-C using the Amaxa Cell Line Nucleofector Kit R (Lonza cat#VVCA-1001) per manufacturer's instructions. HeLa cells were synchronized to early G1 by double thymidine block (0.5 mM, Sigma-Aldrich cat#T9250). After the first block of 22 hours, cells were released for 12 hours, followed by a second thymidine block of 12 hours. Cells were released for approximately 11 hours, which corresponds to early G1, based on our previous reports (Bui et al, 2012; Quénet and Dalal 2014; Bui et al 2017)

Glycerol gradient sedimentation
A total of 2 mL of extracted chromatin was applied to 10 mL of 5 to 20% glycerol gradient containing 50 mM Tris-HCl pH 8.0, 2 mM EDTA, 0.1% NP-40, 2 mM DTT, 0.15 M NaCl, and 1X protease inhibitor cocktail layered over 0.4 mL of 50% glycerol. The chromatin was centrifuged with a SW41Ti rotor (Beckman) at 22,000 rpm for 15.5 hours at 4ºC. 1 mL aliquots were fractioned from the top, and DNA and protein samples were separated by either 1.2% agarose gel electrophoreses or 4-20% SDS-PAGE gels, respectively. Serial N-ChIP was performed on all 12 fractions.

AFM and image analysis
Imaging of CENP-C and CENP-A N-ChIP and bulk chromatin was performed as described (Dimitriadus et al 2010; Walkiewicz et al 2014) with the following modifications. Imaging was performed by using standard AFM equipment (Oxford Instruments, Asylum Research's Cypher S AFM, Santa Barbara, CA) with silicon cantilevers (OTESPA or OTESPA-R3 with nominal resonances of ~300 kHz, stiffness of ~42 N/m, and tip radii of 3–7 nm and FESP with ~75 kHz, 2.8 N/m and 7 nm, respectively, Bruker-Nano) in noncontact tapping mode. Usually, 10 µl stock solution of 4× diluted CENP-C or 10× diluted CENP-A chromatin or 1,000× diluted bulk chromatin was deposited on APS-mica. APS-mica was prepared as previously described (Dimitriadus et al 2010; Walkiewicz et al 2014). The samples were incubated for 10 min, rinsed gently to remove salts, and dried under vacuum before imaging. Images were acquired at high resolution and preprocessed on the NanoScope instrument software.

For the compaction study, we added 1 ng CENP-C^{CD} to purified ACA samples and incubated them for 30 minutes prior to deposition on APS-mica and subsequent imaging. To determine the compaction frequency, we manually counted compacted chromatin clusters based on their size being at least twice as wide as an individual nucleosome, but with an identifiable entry and exit DNA strand.

Automated image analysis was performed as described in (Walkiewicz et al 2014) by using Gwyddion software, NIH ImageJ software (NIH), and R software (instead of Microsoft Excel). A total of six biological replicates were performed for CENP-C experiments and three biological replicates for the CENP-A and bulk chromatin experiments. Bulk chromatin from the same preparation was imaged in parallel to get the baseline octameric range. For all samples, manual spot analyses were performed to confirm accuracy of automated analyses.

Immuno-AFM
In vitro reconstitution of CENP-A (CENP-A/H4 cat#16-010 and H2A/H2B cat#15-0311, EpiCypher, Research Triangle Park, NC) and H3 (H3/H4 cat#16-0008 and H2A/H2B cat#15-0311, EpiCypher Research Triangle Park, NC) nucleosomes were performed as previously described (Dimitriadus et al 2010; Walkiewicz et al 2014). Chromatin from HeLa cells were obtained from fractions 6 and 7 of a glycerol density gradient (containing on average tri-, tetra-, and penta-nucleosome arrays), as fraction 12 did not allow for reliable immune-AFM and subjected these fractions to CENP-C and serial ACA N-ChIP. These samples were subjected to immune-AFM as described previously (Browning-Kelley et al 1997; Cheung & Walker 2008; Banerjee et al 2012). In short, we prepared the samples as followed. First, an aliquot of each sample was imaged by AFM in non-contact tapping mode. Second, the samples were incubated overnight at 4ºC with anti-CENP-A antibody (Abcam cat #ab13939) in an end-over-end rotator. An aliquot of each sample was imaged by AFM in non-contact tapping mode. Third, the samples were incubated with anti-mouse secondary antibody (Li-Cor's IRDye 800CW Donkey anti-mouse IgG cat#925-32212) for an hour at room-temperature in an end-over-end rotator and imaged by AFM in non-contact tapping mode. We analyzed the height profiles of the nucleosomes and antibody complexes as described above.

Force spectroscopy

In vitro reconstitution of CENP-A (CENP-A/H4 cat#16-010 and H2A/H2B cat#15-0311, EpiCypher, Research Triangle Park, NC) and H3 (H3/H4 cat#16-0008 and H2A/H2B cat#15-0311, EpiCypher Research Triangle Park, NC) nucleosomes were performed as previously described (Dimitriadus et al 2010; Walkiewicz et al 2014) CENP-$C_{482-527}$ fragment (ABI Scientific, Sterling, VA) was added in 2.2-fold molar excess to CENP-A nucleosomes. To be able to measure the Young's modulus, the reconstituted chromatin was kept in solution containing 67.5 mM NaCl and 2 mM Mg^{2+} and a different cantilever (Olympus micro cantilever cat# BL-AC40TS-C2. Before each experiment, the spring constant of each cantilever was calibrated using both GetReal™ Automated Probe Calibration of Cypher S and the thermal noise method (Hutter & Bechhoefer 1993). Obtained values were in the order of 0.1 N/m. As a reference to obtain the indentation values, the photodiode sensitivity was calibrated by obtaining a force curve of a freshly cleaved mica surface. All experiments were conducted at room temperature. Force-curves for ~50 nucleosomes for all three conditions were measured using both 'Pick a Point' and force-mapping mode. The maximum indentation depth was limited to ~1.5 nm and the maximum applied force was 150-200 pN. For our analyses, we used Hertz model with spherical indenter geometry for Young's Modulus measurements, $\delta = [3(1 - \nu^2)/(4ER^{1/2})]^{2/3}F^{2/3}$ (for a spherical indenter), where ν is the Poisson ratio of the sample, which is assumed to be 1/3 as in studies reported previously (Radmacher et al 1994; Rakshit et al 2013); δ, F, E, and R are the indentation, force, Young's modulus of the sample and radius of the tip respectively. The radius of the tip was confirmed by SEM and found to be about 10 nm in width.

Transmission electron microscopy

For transmission electron microscopy (TEM), the N-ChIP samples were fixed by adding 0.1% glutaraldehyde at 4ºC for 5 hours, followed by 12-hour dialysis against HNE buffer (10 mM HEPES pH=7.0, 5 mM NaCl, 0.1 mM EDTA) in 20,000 MWCO membranes dialysis cassettes (Slide-A-Lyzer Dialysis Cassette, ThermoFisher cat #66005) at 4ºC. The dialyzed samples were diluted to about 1 µg/mL concentration with 67.5 mM NaCl, applied to carbon-coated and glow-discharged EM grids (T1000-Cu, Electron Microscopy Sciences), and stained with 0.04% uranyl acetate. Dark-field EM imaging was conducted at 120 kV using JEM-1000 electron microscope (JEOL USA, Peabody, MA) with SC1000 ORIUS 11 megapixel CCD camera (Gatan, Inc. Warrendale, PA).

ChIP-exo

Chromatin (digested for 15 min to obtain mostly mononucleosomes) was obtained by serial N-ChIP and the unbound fraction represented bulk chromatin. ChIP-exo was performed as described in (Nikitina et al 2013; Cole et al 2016) with the following modifications. Chromatin was warmed to 30ºC and digested with 0.25 units MNase and 20 units ExoIII for 3 minutes at 30ºC. The digestion was stopped by adding 20 µL 50 mM EDTA and 5% SDS. Subsequently, proteinase K was added to the samples for 1 hours and DNA was extracted by phenol/chloroform and phenol protocol and ran on a 10% Novex TBE gel (ThermoFisher cat #EC6275BOX). The gel was post-stained with Syto 60 (Invitrogen cat #S11342) and imaged with the LiCor's Odyssey CLx scanner and Image Studio v2.0.

ChIP-DNase I

Chromatin (digested for 15 min to obtain mostly mononucleosomes) was obtained by serial N-ChIP and the unbound fraction represents bulk chromatin. ChIP-DNase I was performed as described in (Staynov 2000) with the following modifications. Chromatin was chilled on ice and digested with 50 U of DNase I on ice for 50 minutes. The reaction was stopped by adding 20 mM EDTA and 5% SDS, followed by proteinase K. DNA was extracted by phenol/phenol chloroform extraction and ran on a 10% Novex TBE + urea gel (Invitrogen cat #EC6875BOX). The gel was post-stained with Syto 60 (Invitrogen cat #S11342) and imaged with the LiCor's Odyssey CLx scanner and Image Studio v2.0.

Chromatin fiber immunofluorescence

Chromatin fiber IF was conducted as outlined in Bui et al, 2012. Primary antibodies CENP-C, CENP-A, γH2A.X, and RNAP2 were used at a dilution of 1:500. Alexa secondary antibodies (488, 568 and 647) were used at a dilution of 1:1000, and images were collected using a DeltaVision RT system fitted with a CoolSnap charged-coupled device camera and mounted on an Olympus IX70. Deconvolved IF images were processed using Image J, and co-localization of foci were assessed with its 'Colocalization Finder' plug-in.

Immunostaining of mitotic chromosomes
HeLa cells were synchronized to mitosis with double thymidine block. Primary antibodies CENP-C and CENP-A were used at diluation 1:1000. Alexa secondary (488, and 568) were used at dilution of 1:1000. Images were obtained using DeltaVision RT system fitted with a CoolSnap charged-coupled device camera and mounted on a Olympus IX70. Deconvolved IF images were processed using ImageJ. Mitotic defects (lagging chromosomes and/or multipolar spindles) were counted for 83 and 76 cells (mock, GFP-CENP-C, respectively).

Quench pulse-chase immunofluorescence
To quantify de novo assembled CENP-A particles, we transfected HeLa cells with SNAP-tagged CENP-A (generous gift from Dan Foltz) in combination with either empty vector or GFP-CENP-C using the Amexa Nucleofector kit R (Lonza Bioscience, Walkersville, MD) per instructions. The quench pulse-chase experiment was performed according to Bodor et al 2012. In short, following transfection, cells were synchronized with double thymidine block. At the first release TMR-block (S9106S, New England Biolabs, Ipswich, MA) was added per manufactures instruction and incubated for 30 min at 37ºC, followed by three washes with cell culture media. At the second release TMR-Star (S9105S, New England Biolabs, Ipswich, MA) was added per manufactures instructions and incubated for 15 min at 37ºC, followed by three washes with cell culture media. Fourteen hours after adding TMR-Star, cells were fixed with 1% paraformaldehyde in PEM (80 mM K-PIPES pH 6.8, 5 mM EGTA pH 7.0, 2 mM $MgCl_2$) for 10 min at RT. Next, cells were washed the cells three times with ice cold PEM. To extract solube proteins, cells were incubated with 0.5% Triton-X in CSK (10 mM K-PIPES pH 6.8, 100 mM NaCl, 300 mM sucrose, 3 mM $MgCl_2$, 1 mM EGTA) for 5 min at 4ºC. The cells were rinsed with PEM and fixed for a second time with 4% PFA in PEM for 20 min at 4ºC. Next, the cells were washed three times with PEM. Cells were permeabilized with 0.5% Triton-X in PEM for 5 min at RT and subsequently washes three times with PEM. Next, the cells were incubated in blocking solution (1X PBS, 3% BSA, 5% normal goat serum) for 1 hr at 4ºC. CENP-A antibody (ab13979 1:1000) was added for 1 hr at 4ºC, followed by three washes with 1X PBS-T. Anti-mouse secondary (Alexa-488 1:1000) was added for 1hr at 4ºC, followed by three 1X PBS-T and two 1X PBS washes. Following air-drying, cells were mounted with Vectashield with DAPI (H-1200, Vector Laboratories, Burlingame, CA) and the coverslips were sealed with nail polish. Images were collected using a DeltaVision RT system fitted with a CoolSnap charged-coupled device camera and mounted on an Olympus IX70. Deconvolved IF images were processed using ImageJ and the macro CRaQ (Bodor et al 2012).

ChIP-seq
CENP-C N-ChIP followed by ACA N-ChIP was conducted, as well as an IgG N-ChIP and input control as described above. Next, DNA was isolated by first proteinase K treated the samples, followed by DNA extraction by phenol chloroform. The samples were used to prepare libraries for PacBio single-molecule sequencing as described in manufacturer's protocol (PacBio, Menlo Park, CA). Libraries were produced and loaded on ZWM chip either by diffusion or following size selection of the inserts (> 1000 bp) for all four samples. Subsequently, the reads were sequenced on the PacBio RS II operated by Advanced Technology Center, NCI (Frederick, MD). Sequence reads were mapped to either sequences in RepBase, the consensus sequence used by Hasson et al 2013, and the consensus sequences used by Henikoff et al 2015.

Quantification and Statistical Analyses

Significant differences for nucleosome height measurement from AFM analyses and significant differences for immunostaining quantification, and chromatin compaction quantification, were performed using the t-test as described in the figure legends and main text. Significant differences for the Young's modulus of *in vitro* reconstituted H3, CENP-A, and CENP-A + CENP-C^{CD} were determined using 1-way ANOVA test. Significance was determined at $p < 0.05$.

Supplemental Information

Figures S1-S11 and Tables S1-14

References

Banerjee, S., Arif, M., Rakshit, T., Roy, N.S., Kundu, T.K., Roy, S., & Mukhopadhyay, R, 2012, Structural features of human histone acetyltransferase p300 and its complex with p53, *FEBS Lett*, 586(21):3793-8.

Bodor, D.L., Rodriguez, M.G., Moreno, N., & Jansen, L.E., 2012, Analysis of protein turnover by quantitative SNAP-based pulse-chase imaging, *Curr Protoc Cell Biol*, Chapter 8, Unit 8.

Browning-Kelley, M.E., Wadu-Mesthrige, K., Hari, V., & Liu, G.Y., 1997, Atomic force microscopic study of specific antigen/antibody binding, *Langmuir*, 13(2):343-50.

Bui, M., Dimitriadis, E.K., Hoischen, C., An, E., Quénet, D., Giebe, S., Nita-Lazar, A., Diekmann, S. & Dalal, Y., 2012, Cell-cycle-dependent structural transitions in the human CENP-A nucleosome in vivo, *Cell*, 150(2), pp. 317-26.

Bui, M., Pitman, M., Nuccio, A., Roque, S., Donlin-Asp, P.G., Nita-Lazar, A., Papoian, G.A. & Dalal, Y., 2017, Internal modifications in the CENP-A nucleosome modulate centromeric dynamics, *Epigenetics Chromatin*, 10, p. 17.

Cheung, J.W.C., & Walker, G.C., 2008, Immuno-atomic force microscopy characterization of absorbed fibronectin, *Langmuir*, 24(24);13842-9.

Cole, H.A., Cui, F., Ocampo, J., Burke, T.L., Nikitina, T., Nagarajavel, V., Kotomura, N., Zhurkin, V.B. & Clark, D.J., 2016, Novel nucleosomal particles containing core histones and linker DNA but no histone H1, *Nucleic acids research*, 44(2), pp. 573-81.

Dimitriadis, E.K., Weber, C., Gill, R.K., Diekmann, S. & Dalal, Y., 2010, Tetrameric organization of vertebrate centromeric nucleosomes, *Proc Natl Acad Sci U S A*, 107(47), pp. 20317-22.

Hasson, D., Panchenko, T., Salimian, K.J., Salman, M.U., Sekulic, N., Alonso, A., Warburton, P.E. & Black, B.E., 2013, The octamer is the major form of CENP-A nucleosomes at human centromeres, *Nat Struct Mol Biol*, 20(6), pp. 687-95.

Henikoff, J.G., Thakur, J., Kasinathan, S. & Henikoff, S., 2015, A unique chromatin complex occupies young α-satellite arrays of human centromeres, *Sci Adv*, 1(1).

Hutter, J.L., & Beckhoefer, J., 1993, Calibration of atomic-force microscope tips, *Rev Sci Instrum*, 64(7):1868-73.

Kato, H., Jiang, J., Zhou, B.R., Rozendaal, M., Feng, H., Ghirlando, R., Xiao, T.S., Straight, A.F. & Bai, Y., 2013, A conserved mechanism for centromeric nucleosome recognition by centromere protein CENP-C, *Science*, 340(6136), pp. 1110-3.

Nikitina, T., Wang, D., Gomberg, M., Grigoryev, S.A. & Zhurkin, V.B., 2013, Combined micrococcal nuclease and exonuclease III digestion reveals precise positions of the nucleosome core/linker junctions: implications for high-resolution nucleosome mapping, *J Mol Biol*, 425(11), pp. 1946-60.

Quénet, D., & Dalal, Y., 2014, A long non-coding RNA is required for targeting centromeric protein A to the human centromere, *eLife*, 3:e03254.

Radmacher, M., Fitz, M., Cleveland, J.P., Walters, D.A., & Hansma, P.K., 1994, Imaging adhesion forces and elasticity of lysozyme adsorbed on mica with the atomic force microscope, *Langmuir*, 10(10):3809-14.

Rakshit, T., Banerjee, S., Mishra, S., & Mukhupadhyay, R., 2013, Nanoscale mechano-electronic behavior of a metalloprotein as a variable of metal content. *Langmuir*, 29(40):12511-9.
Shindyalov I.N., Bourne P.E., 1998, Protein structure alignment by incremental combinatorial extension (CE) of the optimal path. *Protein Eng* 11:739-747.
Staynov, D.Z., 2000, DNase I digestion reveals alternating asymmetrical protection of the nucleosome by the higher order chromatin structure, *Nucleic acids research*, 28(16), pp. 3092-9.
Walkiewicz, M. P., Bui, M., Quénet, D. & Dalal, Y., 2014b, Tracking histone variant nucleosomes across the human cell cycle using biophysical, biochemical, and cytological analyses, *Methods Mol Biol* 1170, pp. 589-615

Supplemental Information

Ongoing debate about CENP-A nucleosome conformation and structure

Several important implications arise our observations. First, our data in this report provide insights into the important debate about the conformational and compaction status of CENP-A nucleosomes throughout the cell cycle (Chen et al 2003; Black et al 2004; Fujita et al 2007; Conde e Silva et al 2007; Dalal et al 2007; Williams et al 2009; Bui et al 2012; Wisniewski et al 2014; Kono et al 2015; Nechemia- Arbely et al 2017). AFM measurements of bulk CENP-A nucleosomes from either human or Drosophila cell lines display shortened nucleosomal heights compared to canonical H3 nucleosomes, except at S phase (Dalal et al 2007; Dimitriadis et al 2010; Bui et al 2012; Athwal et al 2015). Our interpretation of these previous data was that *in vivo* CENP-A nucleosomes have a predominantly hemisomal conformation because they contained equimolar ratio of CENP-A, H4, H2A, and H2B. This nucleosomal conformation alters during S phase, where we found that purified CENP-A nucleosomes, which did not contain measurable amounts of H3, became indistinguishable from canonical H3 nucleosomes (Bui et al 2012). We interpreted these data to suggest that a mature octameric conformation of CENP-A nucleosomes is formed at S phase.

In contrast, other reports have recently argued that ectopically over-expressed CENP-A forms octameric centromere-specific nucleosomes (determined primarily by ChIP-seq) based on its wrapping of 100- 120bp of DNA (Hasson et al 2013), or, in a subsequent paper, 133bp (Nechemia-Arbely et al 2017), a value which remains unchanged in G1, G2, and M phase. The interpretation of these ChIP-seq data contradicts earlier *in vitro* and *in vivo* measurements. Both,

data from the crystal structure (Tachiwana et al 2011) and cryo-EM images (Roulland et al 2016) of *in vitro* reconstituted CENP-A nucleosomes show that 10 bp of both the entry and exit DNA of the nucleosomes are disordered compared to canonical H3 nucleosomes, resulting in the protection of no more than ~120 bp by an octameric CENP-A nucleosome. This is consistent with extensive nuclease digestion experiments of *in vivo* purified CENP-A nucleosomes (Yoda et al 2000; Conde e Silva et al 2007; Dalal et al 2007; Dimitriadis et al 2010; Bui et al 2012; Hasson et al 2013; Henikoff et al 2015; Thakur & Henikoff 2016). Another possibility is that the bulk CENP-A nucleosomes which loosely wrap DNA are digested away during the ChIP-seq preparation. While the hemisomal or octameric model, and the compacted/rigid nature of CENP-A nucleosomes remains contested, the innate elastic behavior of CENP-A nucleosomes appears to be an emerging paradigm supported by multiple lines of evidence (Bui et al 2012; Winogradoff et al 2015; Falk et al 2015; Falk et al 2016), including our work here. That said, our immuno-AFM data clearly support the presence of rigidified CENP-A containing octameric nucleosomes within active kinetochore complexes in human cells.

Supplemental Figure Legends

Figure S1. CENP-A nucleosomes display diminished local flexibility when bound to CENP-C^{CD}

(A) The distance between the center of mass (COM) of histone dimers is shown in blue for CENP-A + CENP-C^{CD} and in red for CENP-A. Upon CENP-C^{CD} binding the center of mass of various histone dimer pairs of the CENP-C nucleosome is limited, which means that CENP-C^{CD}

induces a global loss of CENP- A nucleosome flexibility. (B) Residue root mean square fluctuations (RMSF) shows freezing of local flexibility in the CENP-A nucleosome shown in red and with CENP-C^{CD} bound shown in blue. In the region of CENP-C^{CD} binding, the first heterotypic half on the top panel, CENP-C^{CD} is seen to freeze the acidic patch and the loop 1 region of CENP-A. Dashed lines separate individual histones.

Figure S2. CENP-C binds CENP-A, not H3 nucleosomes

(A) Extracted chromatin was digested over a range of time points, (B) resulting in different sized nucleosome array sizes. (C) Chromatin was digested for 2, 6, 10, 30 minutes, followed by CENP-C N-ChIP and the SDS-PAGE gel was stained with safe-blue Coomassie revealing that at 6 minutes and longer digestion histones came down in equimolar ratios. Very short MNase digestion allowed the isolation of soluble CENP-C. (D) Western blotting of chromatin digested at 2, 4, 6, and 10 minutes showed that CENP-A, not H3 or RNA polymerase II, is enriched in shorter array following CENP-C N-ChIP. Medium sized arrays (4 minutes) showed a mixture of H3 and CENP-A, whereas 2-minute digestion allowed isolation of soluble CENP-C.

Figure S3. Both CENP-A population occupy similar centromeric sequences

(A) The obtained PacBio sequences from either the CENP-C N-ChIP or serial ACA N-ChIP first based on their AT content and (B) second on their sequence composition. ALR, ALR1, and ALR2 are alpha satellite DNA from RepBase, Hasson is based on the sequence used by Hasson et al (2013), Henikoff_Cen1 and Henikoff_Cen13 were derived from Henikoff et al 2015.

Figure S4. CENP-C associates with long stretches of DNA

DNA was purified following serial N-ChIP after 6, 15, or 30 minutes MNase digestion and subsequent proteinase K digestion. DNA was purified by phenol/chloroform purification and ran on the 2100 BioAnalyser from Agilent.

Figure S5. Extensive digestion of DNA ends similar between bulk CENP-A nucleosomes and CENP- C associated nucleosomes

(A) To determine how much DNA is wrapped around a nucleosome, a combination of exonuclease III and S1 nuclease was used. Following double digestion, only DNA protected by the nucleosome will remain, assuming that a tight wrapping of DNA around the nucleosome limiting access to the DNA ends by Exo/S1 nucleases. (B) Following double digestion at 30oC with 20 units of exonuclease III and 0.25 units of MNase, DNA was extracted and ran on a 10% TBE gel, allowing for separation of nucleosome- sized DNA fragments. (C) A model of how CENP-C bound to CENP-A nucleosomes result in a weak protection at 20bp from DNA entry and exit, as predicted by (Kato et al., 2013).

Figure S6. Immuno-AFM with Fab confirms specificity of secondary antibody

Height measurements of Fab secondary alone, in complex with CENP-A antibody, and *in vitro* reconstituted CENP-A nucleosome arrays, confirming the specificity of CENP-A antibody.

Figure S7. Bulk chromatin

A collage of TEM and AFM images of (A) H2A N-ChIP or bulk chromatin, (B) CENP-A chromatin, and (C) CENP-C bound chromatin. In the latter example, multiple nucleosomes can

be seen to be associated with the large CENP-C complex, as well as the presence of stretches of nucleosome-free DNA.

Figure S8. CENP-C overexpression did not increase double strand DNA breaks

Representative images of either wild-type or CENP-C overexpressing HeLa cells. HeLa cells were transfected 3 days and synchronized to early G1 prior to fixation and staining for CENP-C, CENP-A, and γH2A.X, a dsDNA break marker. No difference in γH2A.X foci was observed between the two samples.

Figure S9. Two CENP-C^{CD} fragment strengthens rigidification of CENP-A nucleosomes

(A) The distance between the center of mass (COM) of histone dimers is shown in red for CENP-A, blue for CENP-A + 1 CENP-C^{CD}, and in orang for CENP-A + 2 CENP-C^{CD}. Two CENP-C^{CD} fragment exaggerated the COM distances compared to a single CENP-C^{CD} fragment, which means that 2 CENP-C^{CD} further induces a global loss of CENP-A nucleosome flexibility. (B) Residue root mean square fluctuations (RMSF) shows freezing of local flexibility in the CENP-A nucleosome shown in red, 1 CENP-C^{CD} bound shown in blue, and 2 CENP-C^{CD} bound shown in orange. In the region of CENP-C^{CD} binding, the first heterotypic half on the top panel, CENP-C is seen to freeze the acidic patch and the loop 1 region of CENP-A. One CENP-C^{CD} creates asymmetry, especially at the C-terminal end of H2A and H2B, this is abrogated when the second CENP-C^{CD} is bound. Dashed lines separate individual histones. (C) All-atom computational modeling of DNA gyre separation or DNA gyre sliding of CENP-A nucleosome alone or bound to either 1 or 2 CENP-C^{CD} fragments. In each panel, each triangle represents a snapshot from simulation.

Figure S10. Chromatin compaction was altered upon exposure to CENP-C, but CENP-C associated CENP-A nucleosomes remained unchanged.

(A) Representative images of either *in vitro* reconstituted CENP-A nucleosomes with or without CENP-C^{CD}, or *in vivo* extracted ACA N-ChIP from either untreated sample where we added 1 ng CENP-C^{CD}, or WT versus CENP-C OE. (B) Quantification of nucleosomal heights of both elastic and rigidified CENP-A nucleosomes (unbound and bound CENP-A's) in wild-type or CENP-C overexpressing cells in early G1.

Figure S11. Modest decrease in RNAP2 colocalizing to both CENP-C and CENP-A foci

(A) A collage of fiber IF images comparing wild-type and CENP-C overexpressing HeLa cells that were synchronized to early G1 and stained for CENP-A, CENP-C, and RNAP2. For the wild-type HeLa cells, CENP-C:RNAP2 colocalization was determined from 21 fibers and 9 for CENP-A:RNAP2. For CENP-C overexpressed HeLa cells, CENP-C:RNAP2 colocalization was determined from 28 fibers and 15 for CENP-A:RNAP2. (B) Mitotic defects (lagging and/or multipolar spindles) were quantified.

References

Athwal, R.K., Walkiewicz, M.P., Baek, S., Fu, S., Bui, M., Camps, J., Ried, T., Sung, M.H. & Dalal, Y., 2015, CENP-A nucleosomes localize to transcription factor hotspots and subtelomeric sites in human cancer cells, *Epigenetics Chromatin*, 8, p. 2. Black, B.E., Foltz, D.R.,

Chakravarthy, S., Luger, K., Woods, V.L. & Cleveland, D.W., 2004, Structural determinants for generating centromeric chromatin, *Nature*, 430(6999), pp. 578-82.

Bui, M., Dimitriadis, E.K., Hoischen, C., An, E., Quénet, D., Giebe, S., Nita-Lazar, A., Diekmann, S. & Dalal, Y., 2012, Cell-cycle-dependent structural transitions in the human CENP-A nucleosome in vivo, *Cell*, 150(2), pp. 317-26. Chen, E.S., Saitoh, S., Yanagida, M. & Takahashi, K., 2003, A cell cycle-regulated GATA factor promotes centromeric localization of CENP-A in fission yeast, *Mol Cell*, 11(1), pp. 175-87.

Conde e Silva, N., Black, B.E., Sivolob, A., Filipski, J., Cleveland, D.W. & Prunell, A., 2007, CENP-A- containing nucleosomes: easier disassembly versus exclusive centromeric localization, *J Mol Biol*, 370(3), pp. 555-73. Dalal, Y., Wang, H., Lindsay, S. & Henikoff, S., 2007, Tetrameric structure of centromeric nucleosomes in interphase Drosophila cells, *PLoS Biol*, 5(8), p. e218.

Dimitriadis, E.K., Weber, C., Gill, R.K., Diekmann, S. & Dalal, Y., 2010, Tetrameric organization of vertebrate centromeric nucleosomes, *Proc Natl Acad Sci U S A*, 107(47), pp. 20317-22. Falk, S.J., Guo, L.Y., Sekulic, N., Smoak, E.M., Mani, T., Logsdon, G.A., Gupta, K., Jansen, L.E., Van Duyne, G.D., Vinogradov, S.A., Lampson, M.A. & Black, B.E., 2015, Chromosomes. CENP-C reshapes and stabilizes CENP-A nucleosomes at the centromere, *Science*, 348(6235), pp. 699-703.

Falk, S.J., Lee, J., Sekulic, N., Sennett, M.A., Lee, T.H. & Black, B.E., 2016, CENP-C directs a structural transition of CENP-A nucleosomes mainly through sliding of DNA gyres, *Nat Struct Mol Biol*, 23(3), pp. 204-8. Fujita, Y., Hayashi, T., Kiyomitsu, T., Toyoda, Y., Kokubu, A., Obuse, C. & Yanagida, M., 2007, Priming of centromere for CENP-A recruitment by human hMis18alpha, hMis18beta, and M18BP1, *Dev Cell*, 12(1), pp. 17-30.

Hasson, D., Panchenko, T., Salimian, K.J., Salman, M.U., Sekulic, N., Alonso, A., Warburton, P.E. & Black, B.E., 2013, The octamer is the major form of CENP-A nucleosomes at human centromeres, *Nat Struct Mol Biol*, 20(6), pp. 687-95.

Henikoff, J.G., Thakur, J., Kasinathan, S. & Henikoff, S., 2015, A unique chromatin complex occupies young α-satellite arrays of human centromeres, *Sci Adv*, 1(1).

Kono, H., Shirayama, K., Arimura, Y., Tachiwana, H. & Kurumizaka, H., 2015, Two arginine residues suppress the flexibility of nucleosomal DNA in the canonical nucleosome core, *PLoS One*, 10(3), p. e0120635. Nechemia-Arbely, Y., Fachinetti, D., Miga, K.H., Sekulic, N., Soni, G.V., Kim, D.H., Wong, A.K., Lee, A.Y., Nguyen, K., Dekker, C., Ren, B., Black, B.E. & Cleveland, D.W., 2017, Human centromeric CENP-A chromatin is a homotypic, octameric nucleosome at all cell cycle points, *J Cell Biol*, 216(3), pp. 607-21.

Roulland, Y., Ouararhni, K., Naidenov, M., Ramos, L., Shuaib, M., Syed, S.H., Lone, I.N., Boopathi, R., Fontaine, E., Papai, G., Tachiwana, H., Gautier, T., Skoufias, D., Padmanabhan, K., Bednar, J., Kurumizaka, H., Schultz, P., Angelov, D., Hamiche, A. & Dimitrov, S., 2016, The Flexible Ends of CENP-A Nucleosome Are Required for Mitotic Fidelity, *Mol Cell*, 63(4), pp. 674-85.

Thakur, J. & Henikoff, S., 2016, CENPT bridges adjacent CENPA nucleosomes on young human α- satellite dimers, *Genome research*, 26(9), pp. 1178-87. Williams, J.S., Hayashi, T., Yanagida, M. & Russell, P., 2009, Fission yeast Scm3 mediates stable assembly of Cnp1/CENP-A into centromeric chromatin, *Mol Cell*, 33(3), pp. 287-98.

Winogradoff, D., Zhao, H., Dalal, Y. & Papoian, G.A., 2015, Shearing of the CENP-A dimerization interface mediates plasticity in the octameric centromeric nucleosome, *Sci Rep*, 5, p. 17038. Wisniewski, J., Hajj, B., Chen, J., Mizuguchi, G., Xiao, H., Wei, D., Dahan, M. &

Wu, C., 2014, Imaging the fate of histone Cse4 reveals de novo replacement in S phase and subsequent stable residence at centromeres, *Elife*, 3, p. e02203.

Yoda, K., Ando, S., Morishita, S., Houmura, K., Hashimoto, K., Takeyasu, K. & Okazaki, T., 2000, Human centromere protein A (CENP-A) can replace histone H3 in nucleosome reconstitution in vitro, *Proc Natl Acad Sci U S A*, 97(13), pp. 7266-71.

Supplemental Figure S1

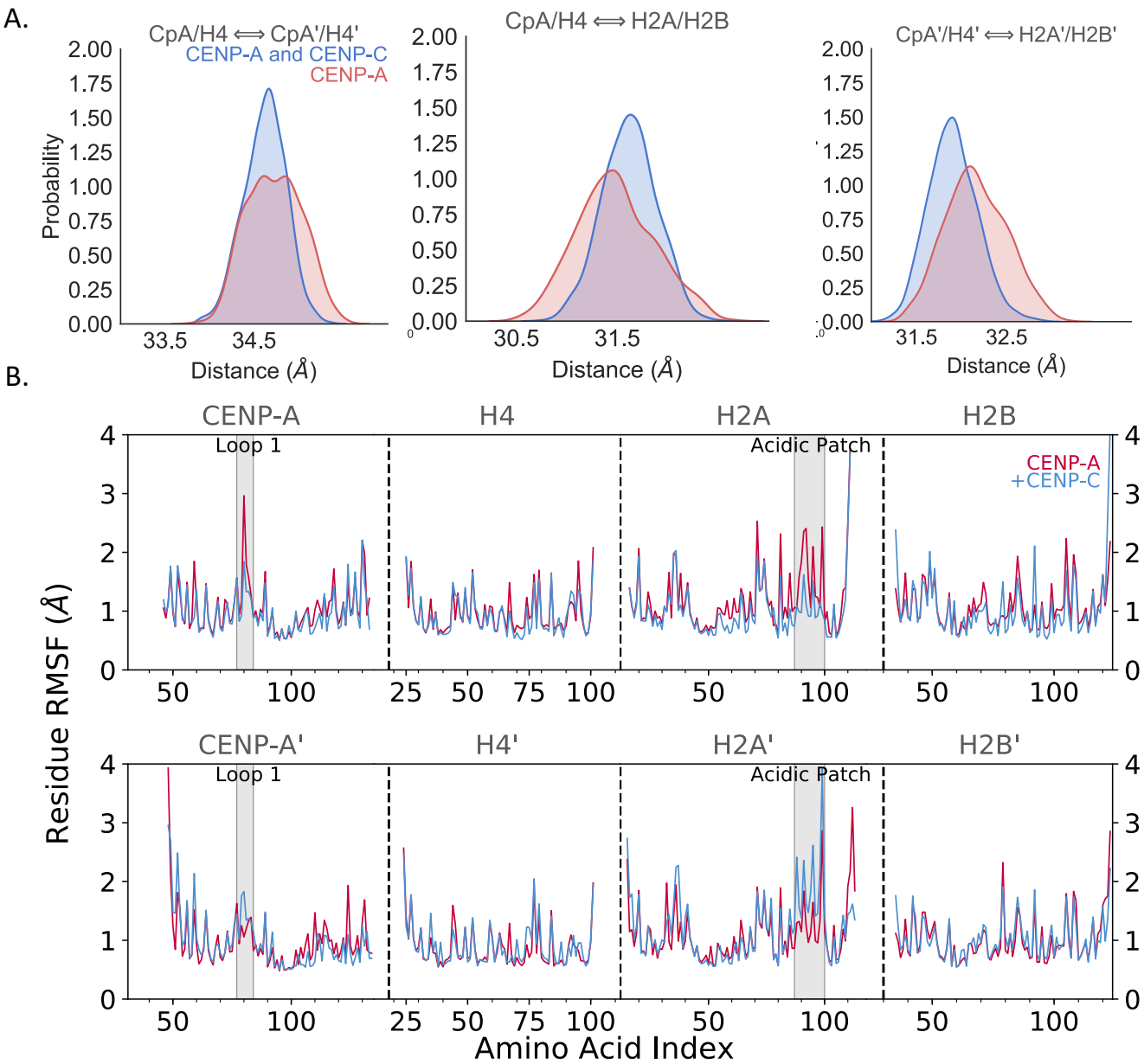

Supplemental Figure S2

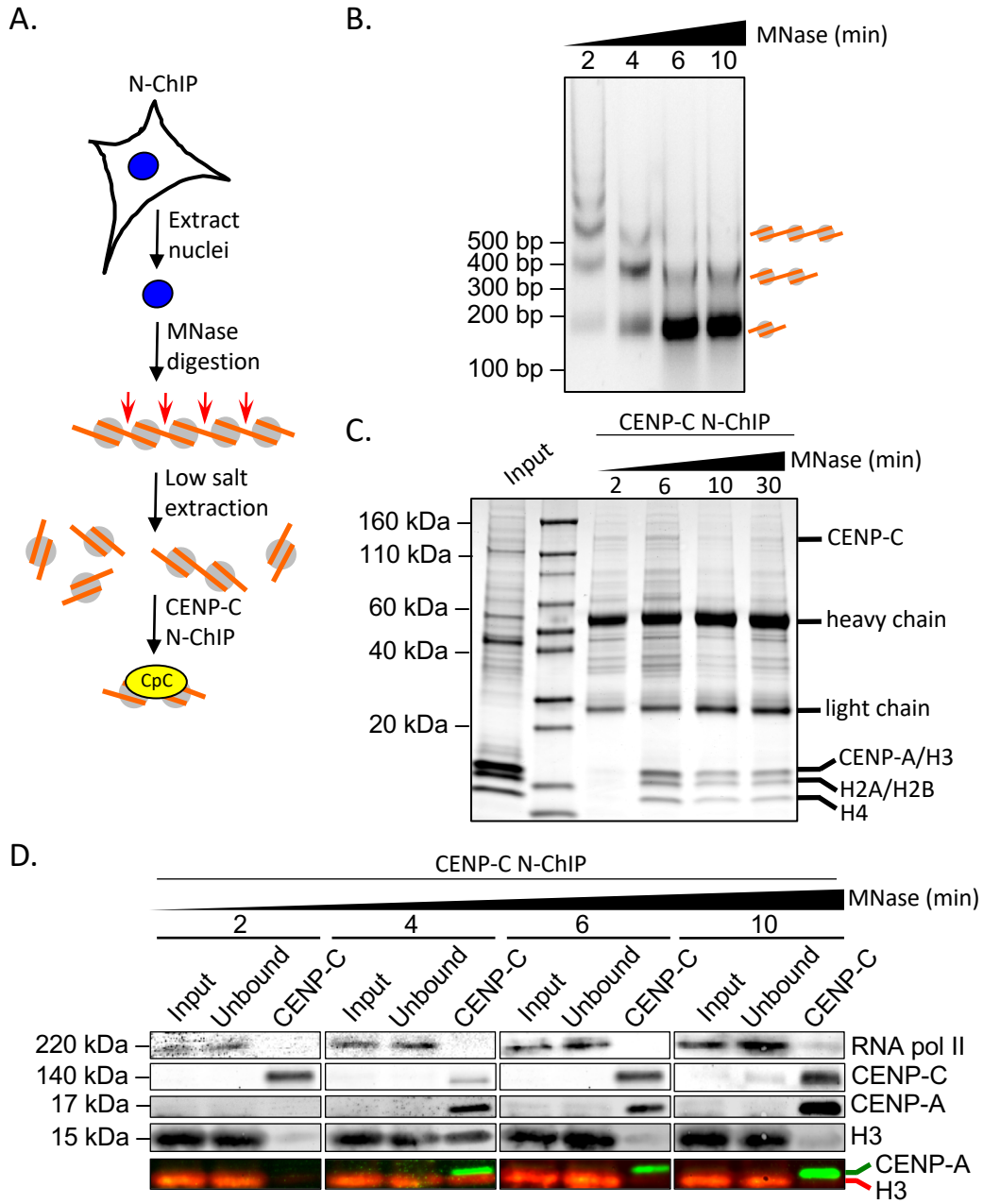

Supplemental Figure S3

A.

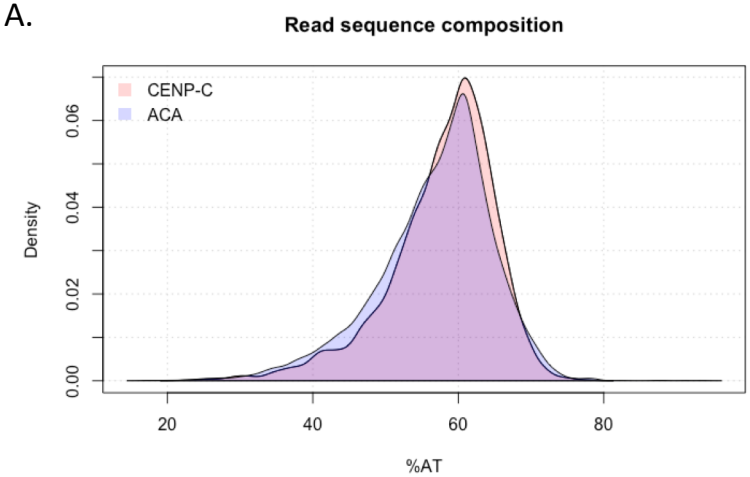

B.

	ACA		***CENP-C***	
Monomers	**Count**	**Fraction**	**Count**	**Fraction**
ALR	35	3.12%	6	2.80%
ALR1	60	5.35%	10	4.67%
ALR2	17	1.52%	12	5.61%
Hasson	457	40.77%	90	42.06%
Henikoff_Cen1	454	40.50%	76	35.51%
Henikoff_Cen13	98	8.74%	20	9.35%
Total	**1121**	**100.00%**	**214**	**100.00%**

Supplemental Figure S4

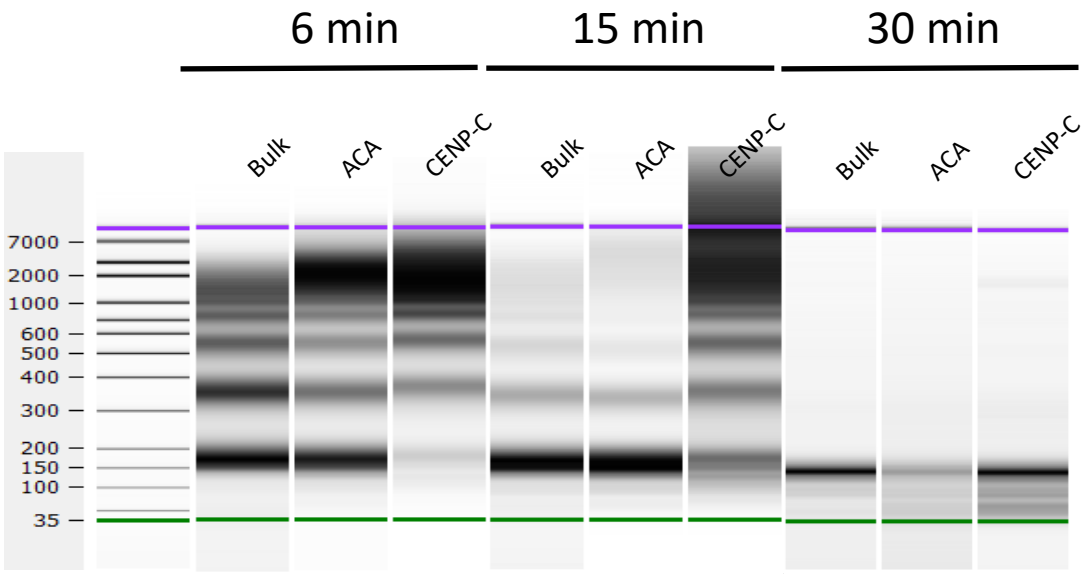

Supplemental Figure S5

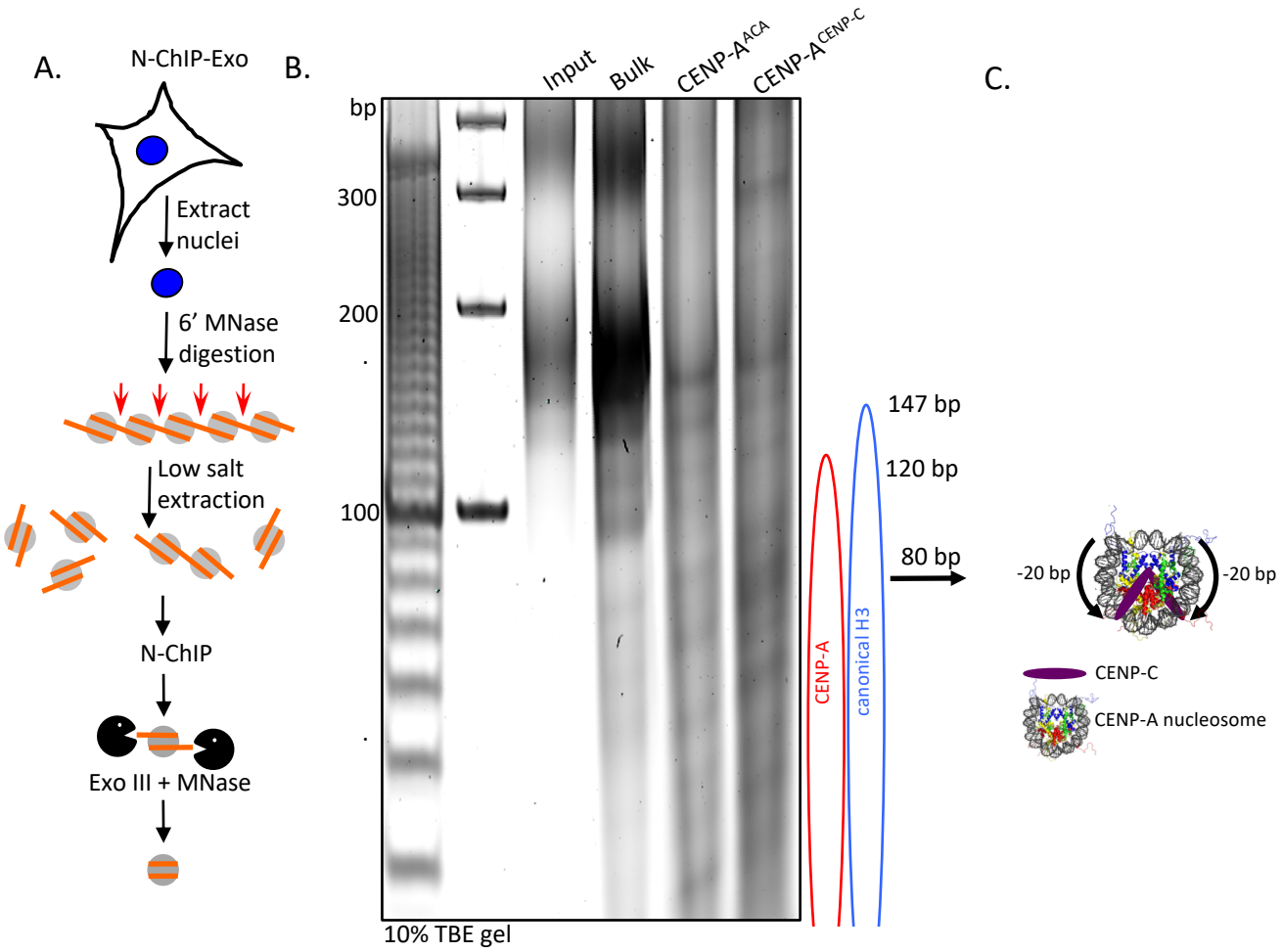

Supplemental Figure S6

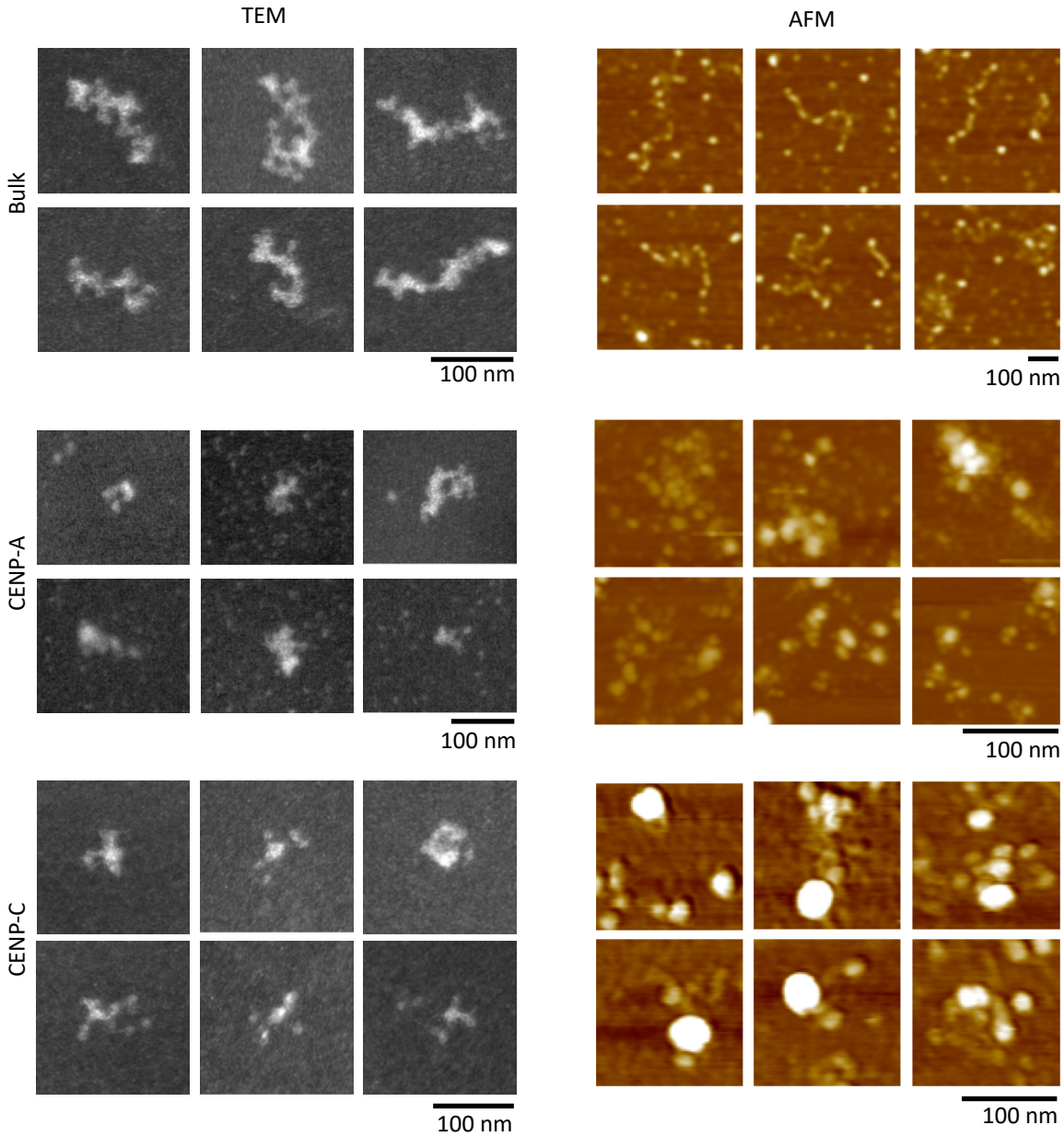

Supplemental Figure S7

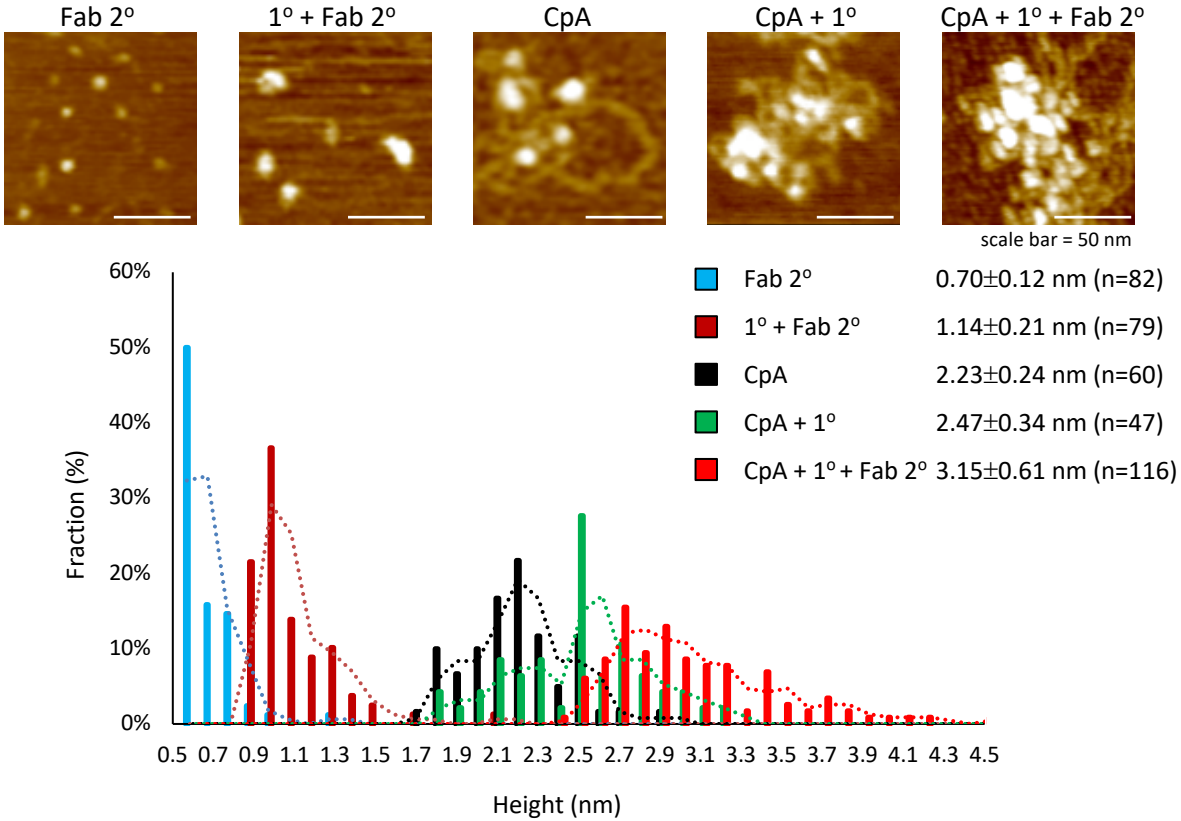

Supplemental Figure S8

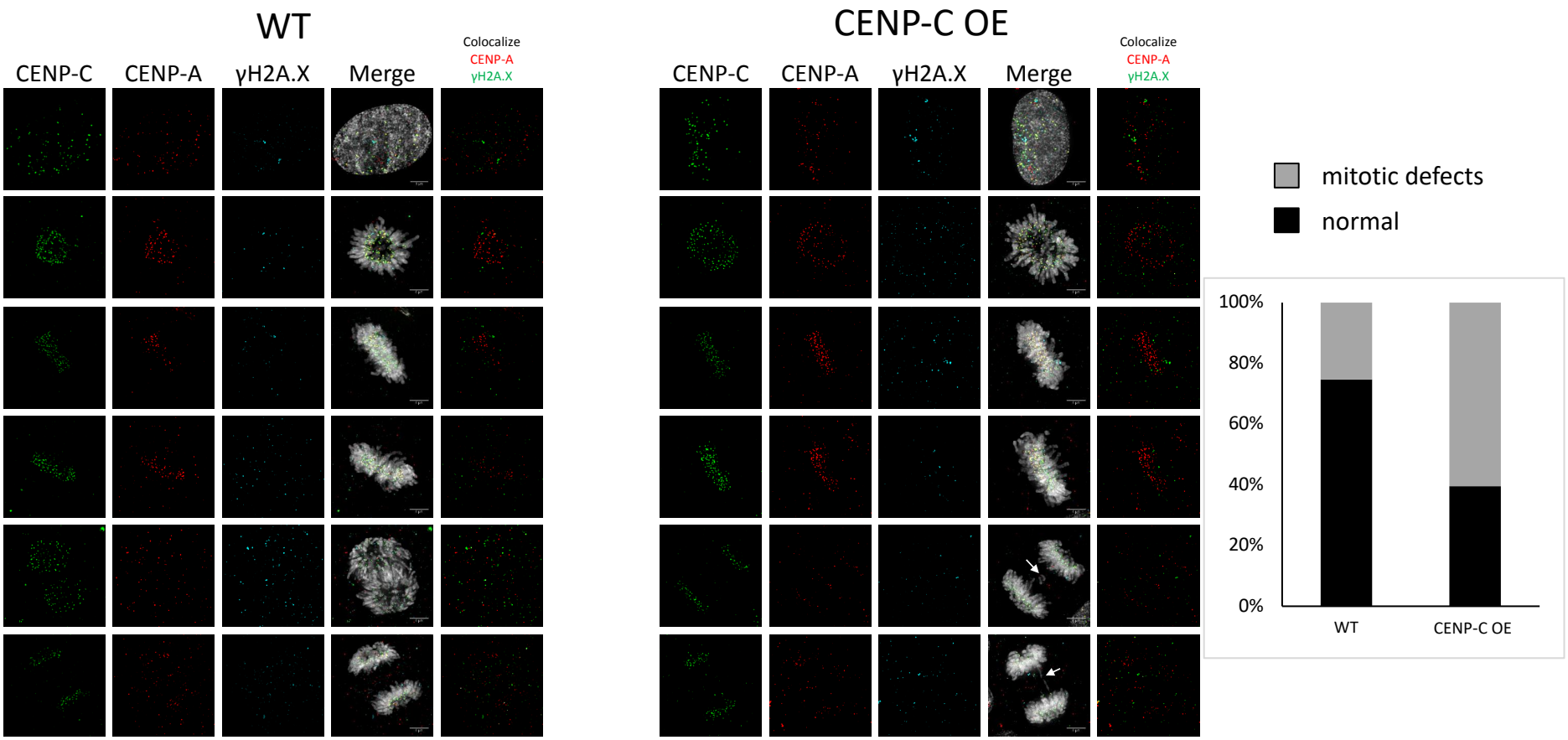

Supplemental Figure S9

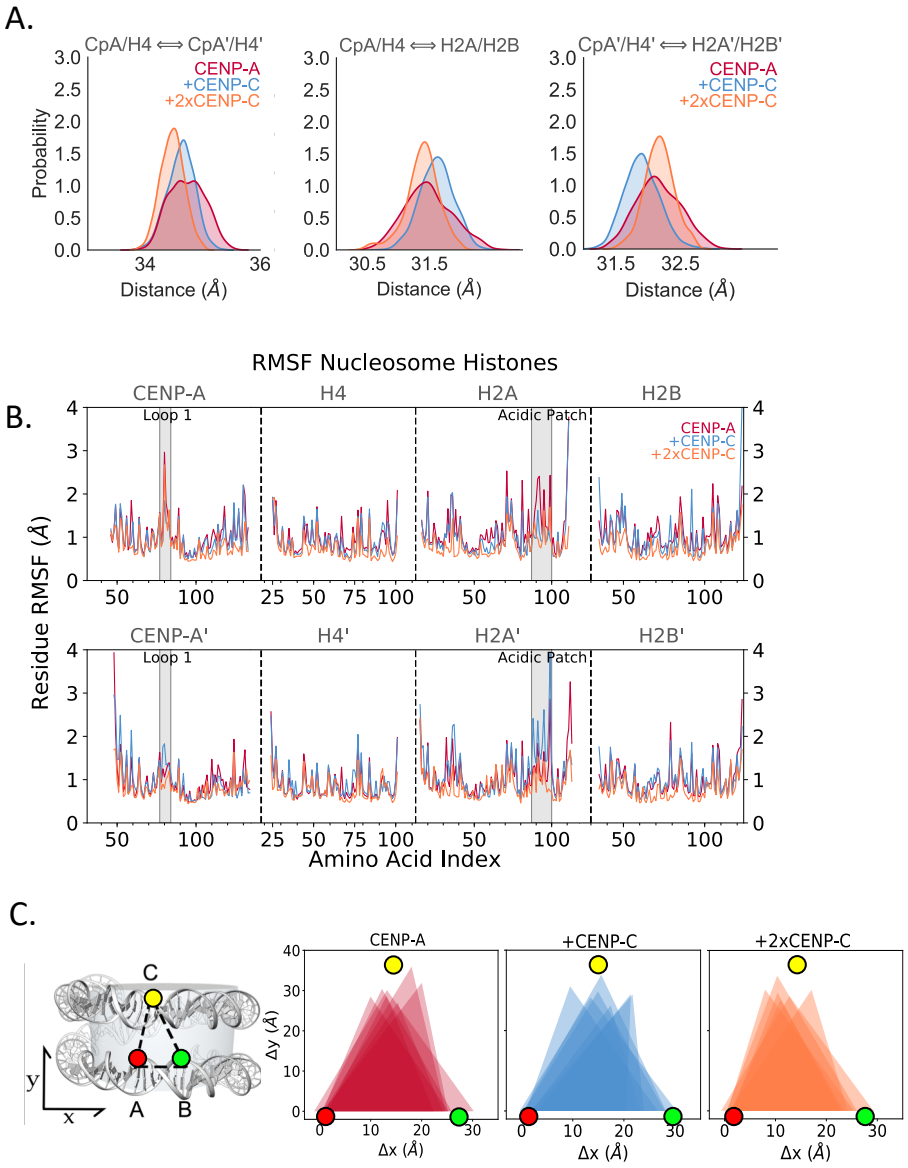

Supplemental Figure S10

A.

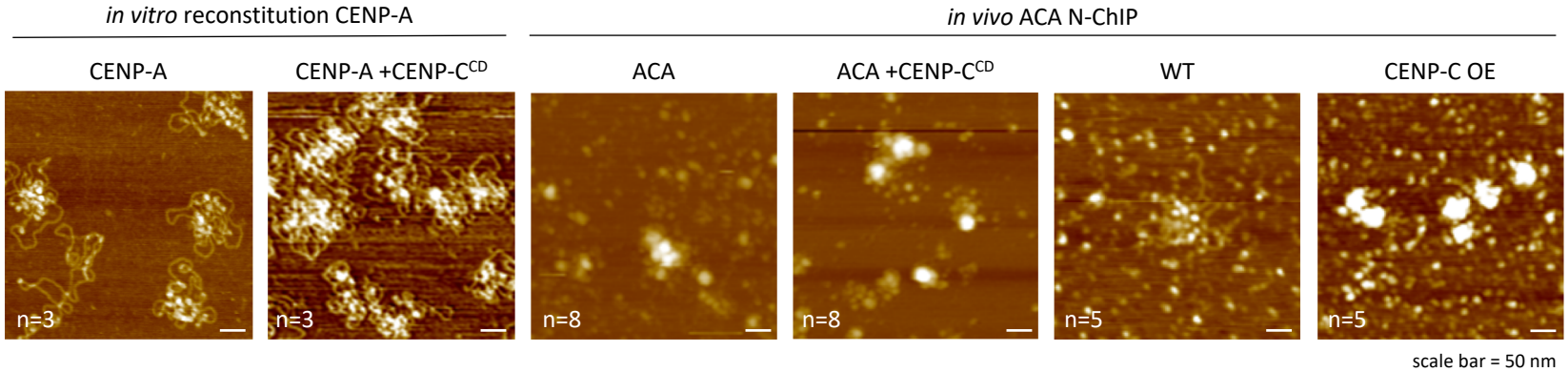

B.

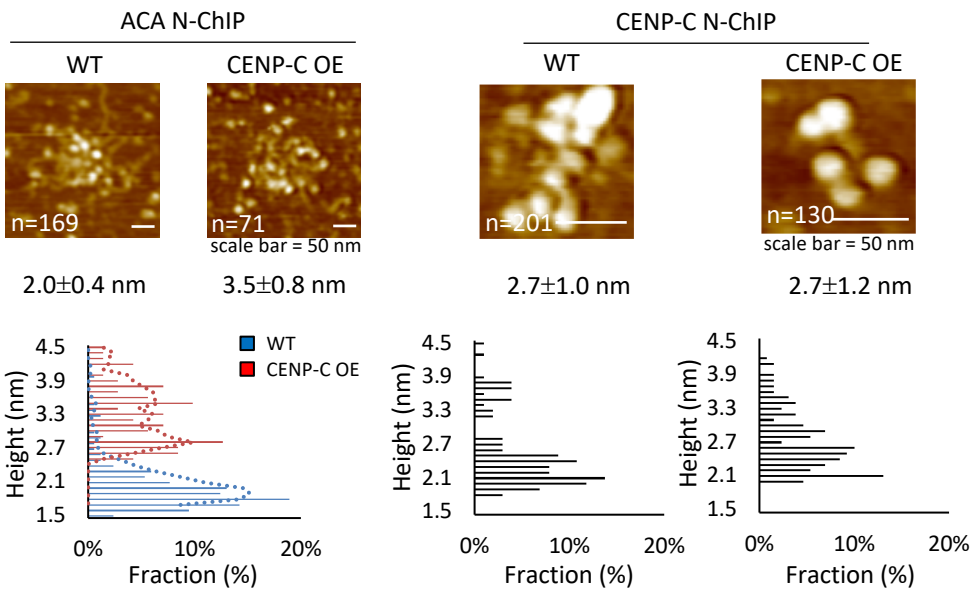

Supplemental Figure S11

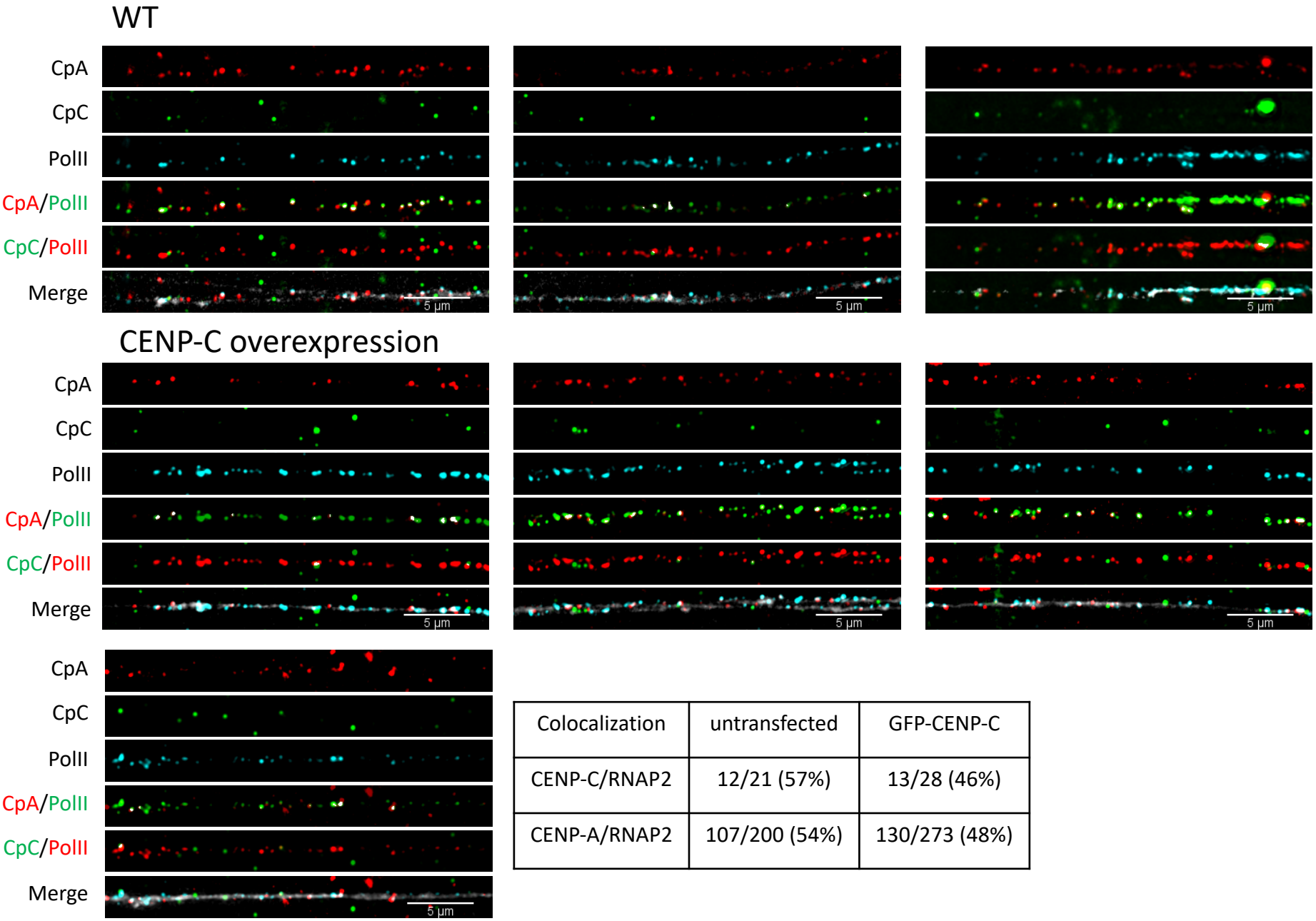

Colocalization	untransfected	GFP-CENP-C
CENP-C/RNAP2	12/21 (57%)	13/28 (46%)
CENP-A/RNAP2	107/200 (54%)	130/273 (48%)